2011

Hydrodynamic focusing micropump module with PDMS/nickel-particle composite diaphragms for microfluidic systems

Jeonghwan Kim
Louisiana State University and Agricultural and Mechanical College, kjeong2@tigers.lsu.edu

HYDRODYNAMIC FOCUSING MICROPUMP MODULE WITH PDMS/NICKEL-PARTICLE COMPOSITE DIAPHRAGMS FOR MICROFLUIDIC SYSTEMS

A Thesis

Submitted to the Graduate Faculty of the
Louisiana State University and
Agricultural and Mechanical College
in partial fulfillment of the
requirements for the degree of
Master of Science in Electrical Engineering

in

The Department of Electrical and Computer Engineering

by
Jeonghwan Kim
B.S., Kyungwon University, Korea, 2007
May 2011

ACKNOWLEDGEMENTS

This thesis research was carried out at the Center for Advanced Microstructures and Devices (CAMD) at Louisiana State University. This research is a part of a Post-Katrina project, supported by Louisiana Board of Regents (LABoR, PKSFI - FRG 1) with cooperation through CAMD, Louisiana State University Health Science Center (LSUHSC), and Advanced Materials Research Institute (AMRI) at University of New Orleans (UNO).

I would like to express my gratitude to all the people who have supported my master thesis. First of all, I want to deeply thank my advisor, Prof. Pratul K. Ajmera and co-advisor, Dr. Yoonyoung Jin for their advice, guidance, and encouragement throughout the course of this work. They have provided a unique opportunity for me to enrich my knowledge in the area of microfluidics and have encouraged me personally in many matters. Also, I would like to express gratitude to my thesis committee member Dr. Theda Daniels-Race for her interest and valuable suggestions.

I am grateful to Dr. Jost Gottert for the opportunity granted to me to work for this research project at CAMD. Special thanks go to my colleague Mr. Kyung Nam Kang in Department of Electrical & Computer Engineering who provided encouragement and support when I was frustrated during the course of my thesis research. I would like to thank Mr. Edward Song for allowing me to use the facilities of BioMEMS and Bioelectronics Laboratory. I am thankful to Dawit Yemane and Sital Tiwari for technical information and for use of the hot embossing machine at CAMD, and to Jason Guy at Center for Biomodular Multi-scale Systems (CBM^2) for the use of micromilling machine. All these people have provided assistance to this work and I am grateful to them.

Above all, I would like to offer my heartfelt thanks to my family for their love and perseverance through these challenging years. Without their support and understanding, this work would not have been possible.

TABLE OF CONTENTS

ACKNOWLEDGEMENTS ii

LIST OF TABLES vi

LIST OF FIGURES vii

ABSTRACT x

CHAPTER 1. INTRODUCTION 1
1.1 Microfluidics 1
1.2 Motivation 3
1.3 Literature Review 5
1.3.1 Micropump 5
1.3.2 Actuation 6
1.3.3 Valve 8
1.4 Research Objective 11

CHAPTER 2. THE DESIGN OF MULTI-FLUIDIC SPEED-MODULATING (MFSM) MICROPUMP BASED ON SIMULATION RESULTS . . 13
2.1 Diaphragm Simulation 17
2.2 Magnet Simulation 19
2.3 Micropump Flow Rate 22
2.4 Prototype Design of Multi-Fluidic Speed-Modulating (MFSM) Micropump 25

CHAPTER 3. THE FABRICATION OF MULTI-FLUIDIC SPEED-MODUALATING (MFSM) MICROPUMP BASED ON THE DESIGN 28
3.1 PDMS/Ni-Particle Composite (PNPC) Diaphragm 28
3.2 Mold Design 32
3.3 Mold Fabrication 33
3.4 Tesla-Type Valve Fabrication 33
3.5 Bonding Process 36
3.5.1 Polydimethylsiloxane (PDMS) to Glass 36

CHAPTER 4. EXPERIMENT AND RESULTS 37
4.1 Diaphragm Characterization 37
4.1.1 Diaphragm Displacement Measurement 39
4.1.2 PDMS Diaphragm Measurement and Simulation Model 41
4.1.3 Displacement Measurement on PNPC Diaphragm 42
4.1.4 Mechanical Property Measurement of PNPC Diaphragm . . . 44

4.2 MFSM Micropump Module for Hydrodynamic Focusing 47

CHAPTER 5. SUMMARY, CONCLUSION, AND SUGGESTIONS FOR FUTURE WORK 57
5.1 Summary and Conclusions 57
5.2 Suggestions for Future Work 59

REFERENCES 63

VITA 66

LIST OF TABLES

1.1 Definitions of various valves and their advantages and disadvantages. 9

2.1 Nozzle-diffuser equations for low Reynolds number. 23

2.2 Diodicity vs. Reynolds number comparison between nozzle-diffuser and Tesla-type valve. 24

3.1 Tesla-type valve diodicity simulation data based on the design shapes. 35

4.1 Weight percent comparisons obtained from initial ingredient used with the values measured on the fabricated diaphragms. 43

4.2 The PNPC diaphragm (left, middle and right) displacement as a function of the permanent magnet distance from the top of the cover layer to the undisplaced diaphragm under approximate average 1.8 kPa air pressure. 55

LIST OF FIGURES

1.1 Optimized designs of nozzle-diffuser and Tesla-type valves. 10

2.1 (a) A modular microfluidic stack, (b) the initial concept of the MFSM micropump proposed in this work, and (c) system assembly. 15

2.2 Channel modulation with hydrodynamic focusing method utilizing a permanent magnet. 16

2.3 The schematic of the object loaded diaphragm. 18

2.4 Permanent magnet (2 mm dia x 1 mm height) and its magnetic field. (a) Magnetic field (2-D simulation), (b) magnetic field along the X-axis, and (c) magnetic field along the Y-axis. 20

2.5 (a) The magnet and PNPC diaphragm positions for magnetic net force. (b) Net force on the diaphragm of 5 mm diameter as a function of distance due to the permanent magnet. The distance is measured along y-direction in Fig. 2.4. 21

2.6 Conventional pump operation with a nozzle-diffuser structure. (a) Supply mode and (b) pump mode. 23

2.7 Tesla-type valve (a) simulation and (b) diodicity. 26

2.8 MFSM micropump drawing and schematic with (a) oblique view, (b) front cross-sectional view, and (c) plan view of channels in the bottom PDMS layer. . . 27

3.1 Scanning electron microscope (SEM) images of the submicron nickel particles. . . 29

3.2 PDMS/Ni-particle composite (PNPC) diaphragm fabrication procedure. 30

3.3 PNPC diaphragms (a) with 20 wt% and (b) with 40 wt% of nickel particles. Microscope views of (c) 20 wt% and (d) 40 wt% nickel composition cases. Note particle agglomeration in (d). 31

3.4 MFSM micropump designs with varying channel width and chamber diameter values. 32

3.5 (a) MFSM micropump brass mold obtained by micro-milling. (b) Zoomed in view of details on a chip area. 33

3.6 The milling machine limitation effect on the structures. (a) The optimum design shape of the Tesla-type valve and (b) the Tesla-type valve obtained with the milling machine used. 34

3.7 Tesla-type valve fluidic simulation on ANSYS. 35

4.1 (a) Schematic of the nickel particle implanted diaphragm displacement measurement setup. (b) Optical microscope focusing with no applied pressure and (c) optical microscope focusing with applied pressure. 38

4.2 (a) The schematic of the test jig and its pictures in (b) oblique and (c) top view. . . 39

4.3 The photograph of the measurement setup. 40

4.4 The comparison of the measured and simulated PDMS diaphragm displacement. 42

4.5 The measured displacement of diaphragms formed from 29.74 wt% and 29.16 wt% PDMS/Ni-particle composite diaphragms. 44

4.6 Indentation measurement. (a) Indentation equipment setup, (b) front view, and (c) side view of the measurement state, scope, and the loading tip. 45

4.7 Indentation measurements on PDMS/Ni-particle composite diaphragm (29.74 wt% of nickel). (a) Mechanical characteristic data and (b) data analysis of elasticity E_r and hardness H values for 29.74 wt% PNPC diaphragm. 46

4.8 Pictures of the fabricated prototype MFSM micropump module. (a) Top view and (b) details of the feed-throughs for external connections. 48

4.9 The experimental setup for testing the MFSM micropump. 48

4.10 MFSM micropump module test setup. 49

4.11 The schematic of the hydrodynamic focusing channel modulation. (a) Middle focusing with no modulation, (b) right focusing with right diaphragm modulation, and (c) left focusing with left diaphragm modulation. 50

4.12 Channel modulation by a magnetic force on the impregnated nickel particle diaphragm. (a) Middle focusing with no modulation and (b) right focusing with right diaphragm modulation. 52

4.13 Magnetic field as a function of vertical distance from the magnet center. . . . 53

4.14 The PNPC diaphragm displacement by the permanent magnet as a function of the magnet distance from the top of the cover layer to the diaphragm with the approximate average 1.8 kPa applied air pressure. 55

4.15 Measured channel width variations resulting from permanent magnet distance variation from the undisplaced PNPC right diaphragm for approximate average 1.8 kPa air pressure. 56

5.1 Hot embossing process with (a) brass mold inset mounted and (b) PMMA wafer of MFSM micropump obtained after hot embossing. 62

5.2 Structural views of MFSM micropump made in PMMA. 62

ABSTRACT

In this research, a rapid prototype of multi-fluidic speed-modulating (MFSM) micropump which enables modulation of hydrodynamic focusing in micro-fluidic flow has been designed, fabricated, and characterized. The size of the entire module is 33 mm x 25 mm x 8 mm and comprises of three MFSM micropumps to achieve hydrodynamic focusing. These pumps are simultaneously operated by the same actuation source. Each micropump consists of Tesla-type valves in the bottom layer and PDMS/Ni-particle composite (PNPC) diaphragm in the middle layer. The deflection of the diaphragm is obtained by the external pneumatic force, and the permanent magnet controls the displacement resulting from interaction between the magnetic field and the PNPC diaphragm. Analyses of the magnetic modulation force, the flow rate of the MFSM micropump, and the hydrodynamic focused channel modulation are presented. The individual micropump can pump DI water at flow rate of 107 μl/min, and the combination of the three micropumps is able to make the flow rate of 321 μl/min within a hydrodynamic focusing channel. This research successfully examines the possibility of modulation of a neighboring channel flow rate through interaction with a magnetic force field to achieve hydrodynamic focusing of flow in the central channel. With appropriate magnetic interaction with diaphragm, the central channel flow width can also be varied. This technique can be utilized for possible application in drug delivery system (DDS), lab-on-a-chip (LOC) or micro total analysis system (μTAS), and in a point of care testing (POCT) system.

CHAPTER 1

INTRODUCTION

1.1 Microfluidics

Microfluidic technology deals with fluids in micro-domain regarding volume, dimension, power consumption, and so on. This technology since its first appearance in 1950 has enabled miniaturization, integration, and automation of assays to improve experimental throughput by utilizing small amounts of samples or reagents [1-3].

Microfluidic technology has been an integral part of an intensive research and development effort in nanotechnology during the last ten years [4]. Advanced technologies in biological micro-electro-mechanical system (BioMEMS) are supporting the trend to integrate nanometer scale materials and microstructures with microfluidics [4, 5]. Development in bio-medical application technology has been advanced by converging microfluidics with nanotechnology such as nanowires, carbon nanotubes, and nanoparticles. Nanowires and nanostructures also have a great potential to provide point of care testing (POCT). For POCT and other biomedical application including certain BioMEMS, precise detection and quantification of target diseases are critical. Nanowires and nanostructures can potentially increase the sensitivity and selectivity of the sensors [6]. Moreover, nanowire and nanostructure based sensors are label-free, which utilize a direct detection method without attachment of fluorescent, radioactive, or other target specific detector for a real-time direct detection. These benefits from nanowires and nanostructures can significantly improve disease detection capability [7]. The combination of nanotechnology and microfluidics technologies needs addressing of research issues such as chip assembly, cost, accuracy, and integration at nano/micro/macro scale.

The merging of nanotechnology with microfluidic enables promising biomedical applications such as drug delivery system (DDS), lab-on-a-chip (LOC) or micro total analysis system (μTAS), and POCT [8].

Drug delivery system (DDS) is a method to deliver medicine and drug to the location where it is needed in the body. Drug delivery system is one of the most promising areas for using microfluidic technologies involving micropumps, microsensors, and microfluidic channels which interface with nano- and micro- technologies. The system, implanted in the body of a patient having a chronic disease, has to automatically and accurately control the volume of the delivered drug dose. Precise computation is required to establish accurate dose control in a drug delivery system [9].

LOC or μTAS devices involve integration and miniaturization of laboratory functions and processes in chip scale technology. These systems are designed for pretreatment, and for analysis and detection of diseases. The latter requires high accuracy and sensitivity for analysis and measurement. The concept of miniaturization is faced with the challenges and limitation in performance due to extremely small sizes of pumps, valves, and detection systems employed. [8]

POCT can be described as a user friendly diagnostic test, where the test kit can be easily used in patients as a pretest. The test involves sampling a small amount of the urine and/or blood to enable a patient to monitor and manage his or her disease. The convenience must be accompanied by accuracy for reliable management of the disease. An efficient fluidic transport system is an important part of a POCT. A conventional device such as a pump is physically and technically difficult to integrate with the POCT chip despite its reliable performance history [10].

POCT diagnosis has a potential market worth billions of dollars [5]. The U.S projected POCT market was $2.13 billion by Frost & Sullivan in 2009, and it is estimated to grow to $3.93

billion in 2016 [11]. The advantages of POCT include cost effectiveness, small size, convenience of portability, and fast response time for testing of urine and blood. Many research areas need further development to obtain a complete POCT chip involving nanotechnology and microfluidics. These areas include reduction in chip dimension, development in chip assembly technology, cell agglomeration, system integration methodologies, and many others. Development of a microfluidic chip with low cost and reliable performance currently still needs significant efforts.

1.2 Motivation

Several issues need to be addressed in order to apply microfluidic systems *in vivo*. These include power consumption [12], cell agglomeration, channel alignment [13], sensitivity [14], and manufacturability. Among them, one important issue is controlling the flow of micro fluids. The current trends in BioMEMS include smaller sample volume, portability, integration with other microfluidic devices and accuracy [15], low cost, and high performance.

In general, there is an inverse tradeoff between the size and the cost of the device. For instance, the alignment cost of the chip using nanometer-size channels increases readily. Nanostructures such as nanowires, carbon nanotubes, and nanoparticles provide several advantages such as smaller sample volume, decrease in chip size, and improved accuracy. Though a larger channel width reduces the alignment cost, it also increases the reaction uncertainty between the functionalized structure and the target cell due to the wider channel size. The other issue is that cell agglomeration can easily block channels [16], when the sample cells are made to flow through a narrow channel. Hydrodynamic focusing method is a possible solution to protect against cell agglomeration [17].

Hydrodynamic focusing method helps in reducing alignment cost since the method does not necessarily require a narrow channel. In hydrodynamic focusing method, the width of the middle stream is controlled by the flow rate of the two buffer streams present on either side of the middle channel. Thus, the width of the middle channel flow containing the sample of interest can be narrowed to nanosize by adjusting the adjacent channel flow rates. In addition, the hydrodynamic focusing method utilizing three pumps to control the flow rates is able to retain high sensitivity. Three pumps utilized in the hydrodynamic focusing method can adjust the location of the middle stream of the channel by modulating the flow rates of the pumps. Thus, the middle channel containing the test samples can be made to move from one side to the other side of the channel permitting behavior achievable in a nanostructure device while utilizing a wide-channel device.

However, a syringe pump, which is a commonly used pump by current researchers on microfluidics systems, is bulky and needs a complex controller unit and is not easily portable. Hence, hydrodynamic focusing method, which needs three pumps, can only be readily employed in a laboratory setting. It is hence necessary to reduce the overall size of the pump and to eliminate its control unit for its use in a LOC or a POCT device.

A multi-fluidic speed-modulating (MFSM) micropump based on the hydrodynamic focusing method is proposed here to overcome these challenges. MFSM micropump is a possible solution that permits sensors employed in POCT and LOC devices retain their benefits. The micropump enables a hydrodynamically focused channel utilizing three micropumps. The module is able to control the position of the hydrodynamically focused channel by manipulating diaphragm displacements with magnetic force. The feature size of the module is much smaller (several millimeters in length and width) than a typical syringe pump. MFSM micropump

consumes less power compared with other micropumps. MFSM micropump is operated by external air pressure as the driving source. Due to its overall small size, the device will be highly portable and suitable for many applications. In order to realize the prototype MFSM micropump module, its actuation method and its components are studied here. Furthermore, each component of the micropump is examined critically to arrive at a suitable and appropriate prototype design.

1.3 Literature Review

The current micropump technologies are summarized here along with the general subcomponents of a micropump such as actuator, chamber, and valve. An optimum micropump design can be achieved by studying its working principle and performance. The study of subcomponents of the micropump can provide a basis for a new micropump design.

1.3.1 Micropump

Micropumps for Micro-Electro-Mechanical Systems (MEMS) have been researched for a couple of decades. The pumps having micro-metric dimensions deal with small amount of flow volumes in the order of μl/min to ml/min. In addition, micropumps can be utilized in biomedical applications such as disposable drug delivery system [18] and miniaturized total chemical analysis system [19].

Micropumps can be divided into two categories: 1) a periodic or non-continuous micropump or 2) a continuous micropump. Periodic micropumps utilize a periodically driven force from an actuator. Depending on this actuating force, the displacement of the diaphragm changes the volume of the fluid container resulting in a fluidic flow through the inlet and outlet valves. A periodically applied force results in a discontinuous fluid flow. In continuous

micropumps, energy is applied continuously to boost the velocities of the fluid. Examples of continuous pumps include a centrifugal pump, electrohydrodynamic (EHD) pump, electroosmotic (EO) pump, and magnetohydrodynamic (MHD) pump. In addition, sound wave effects depending on the wavelength can also generate fluid flow resulting in an acoustic/ultrasonic pump [20, 21].

A common displacement micropump comprises of a reciprocating diaphragm. The pump consists of a chamber, an inlet, an outlet, and a diaphragm. The diaphragm oscillation results in a volume change of the chamber, so the amount of fluid flow depends on the change of the volume. The diaphragm allows the fluid into the chamber through the inlet valve and pushes the fluid out of the chamber through the outlet valve. For effective actuation piezoelectric, thermopneumatic, electrostatic, and pneumatic pumps are used as a driver.

1.3.2 Actuation

Actuator is necessary to operate the diaphragm of the micropump. There are mainly two types of actuators: external and integrated actuators. An external actuator can generate relatively large force on the diaphragm producing larger deflection. However, sizes of external actuators are normally large and that is a critical disadvantage when micrometer-size pumps are desired. On the other hand, integrated actuators are quite small and have a fast response time. Thus, they are utilized in micropumps. However, small size can be a drawback in generating a large stroke volume. Common types of actuators for diaphragm reciprocation are piezoelectric, thermopneumatic, electrostatic, and pneumatic [20, 22]. Choice of proper actuation type is important and depends on the purpose for which the micropump is to be used. The micropump performance is highly dependent on this choice.

Piezoelectric actuation uses piezoelectric material such as lead-zirconium-titanate (PZT) to yield mechanical strain by an external electric field. Depending on the applied electric field, the piezoelectric material shrinks or expands its geometry in the lateral dimension. Piezoelectric material needs to be integrated directly on the diaphragm of the micropump because of its relatively small movement even though a high voltage is applied. Direct integration makes the fabrication process complex for mass fabrication at a low cost [23].

The fundamental concept of electrostatic actuation uses Coulomb's law between two plates. One of the two plates is the movable part which acts as the pump diaphragm. Electrostatic force is inversely proportional to the square of the distance between the plates and is proportional to the voltage. Thus, small gap and high voltage is frequently necessary for appropriate actuation. The micropump operation by electrostatic actuation is similar to other reciprocating micropumps except for the structural difference in utilizing an electrostatic force. As the voltage applied to the two electrode plates turns on and off, the movable diaphragm is deflected and released. Therefore, the diaphragm forces fluidic flow in and out through the inlet and outlet valves through displacement of the stroke volume within the chamber.

Pneumatic actuation generally uses compression and expansion of air. Externally applied pneumatic force is quite attractive since relatively larger stroke volume can be achieved compared to other actuating methods in spite of difficulty in achieving integration [24]. Thermo-pneumatic actuation, on the other hand, uses air compression and expansion by a heater and it can be integrated in the micropump because of its small size. However, it is not possible to oscillate the diaphragm as much compared to an external pneumatic actuator.

1.3.3. Valve

For better micropump performance, valves are one of the important parts in order to obtain unidirectional fluid flow. There are two available forms of valves: active and passive. Table 1.1 summarizes the definition, advantages, and disadvantage of each valve type. Active valve has a dynamic structure which is operated by an actuator to open and close the valve. Passive valves offer unidirectional flow by deformation or deflection and are classified into two categories. One has dynamic geometry with a movable part but does not require external activation energy. The energy for activation is derived from the fluid flow itself. The valve contains moving structures that helps unidirectional flow by deformation, motion, or deflection. The other type has static and fixed geometry with no movable part in the valve structure. Flow rectification occurs due to unique valve structure such as a nozzle-diffuser or a Tesla-type valve. Since, the static and fixed geometry type has no movable parts, they are preferred for applications involving relatively large particles and cells as the latter have difficulty passing through a movable element. Some dynamic active valves and dynamic geometry passive valves have disadvantages of wear and fatigue and require complex fabrication steps. On the other hand, static and fixed geometry passive valves are beneficial due to their simplicity, low risk of failure, and no clogging. Thus, Static and fixed geometry valves are widely accepted for micropump design. [20, 25, 26]

Nozzle-diffuser and Tesla-type valves are common types of static and fixed geometry valves for micropumps. The valve geometries in these cases rectify fluidic flow due to pressure drops instead of moving parts [27]. Using computational fluidic dynamics (CFD) simulation, nozzle-diffuser and Tesla-type valve designs can be optimized as shown in Fig. 1.1. The CFD

Table 1.1 Definitions of various valves and their advantages and disadvantages. After references [20, 25, 26].

	Active valve	Passive valve		Valveless
	Active Dynamic	Dynamic geometry	Static and fixed geometry	
Definition	Structure that requires energy (electrical, thermal, etc) for flow rectification.	Structure that provides unidirectional flow by deformation, motion or deflection without requiring an external power source.	Components providing flow directionality but no moving part. Example: nozzle-diffuser and Tesla-type valve.	No components providing flow directionality. The pumping mechanism has inherent directionality.
Advantages	▪ high performance ▪ versatility	▪ physical barrier to reverse flow ▪ endures large back-pressure	▪ no moving parts ▪ simple design ▪ low risk of failure ▪ no clogging with the fluids that contains cells or other materials	
Disadvantages	▪ high pressure drop ▪ wear and fatigue of movable parts ▪ high cost due to fabrication complexity ▪ shorter life time ▪ lower reliability	▪ fatigue failure in long-life operation ▪ sticking problem ▪ inherent structure response time (determines operating frequency)	▪ flow failure ▪ no bi-directional flow	

Nozzle-diffuser	Tesla-type valve
Oblique views	
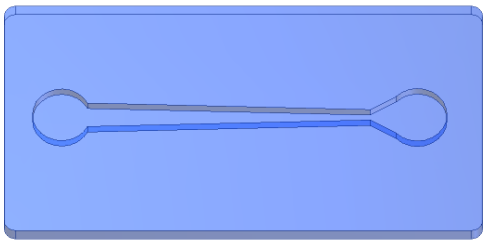	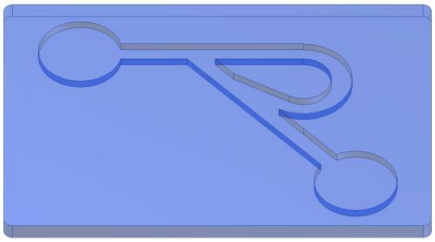
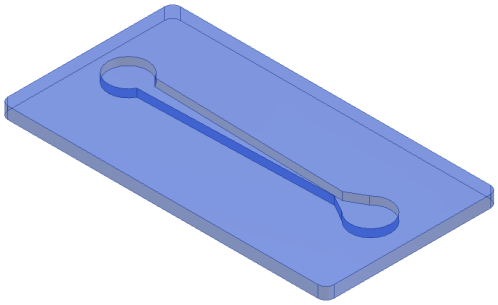	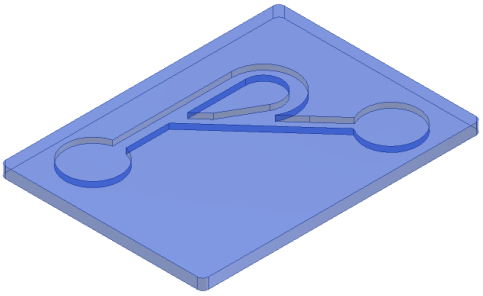

Fig. 1.1 Optimized designs of nozzle-diffuser and Tesla-type valves. After reference [28].

computer modeling can improve rectifying percent for each valve. In general, the diodicity of the Tesla-type valve achieves better performance [28].

1.4 Research Objectives

The goal of this research is to i) build a prototype multi-fluidic speed-modulating (MFSM) micropump module, which makes channel flow modulation possible by a hydrodynamic focusing method, and to ii) test its feasibility in channel modulation by controlling pumping volumes of individual micropumps.

Individual micropumps are first developed, and a novel PDMS/Ni-particle composite (PNPC) diaphragm is invented for the pump. At the same time, a structural module design and its assembly steps are studied. This research is limited to building a prototype design for modulation of fluid flow in a channel.

The following chapters give the details of the approach used to build the prototype design. The computation design of the MFSM micropump module is given in chapter 2. The fabrication process is described in chapter 3. The experimental setup and test of the assembled module is given in chapter 4, and the summary and conclusions are given in chapter 5.

In chapter 2, the computational simulation for MFSM micropump design is discussed, and the simulation is performed for individual components of the MFSM micropump. The simulation result provides guidelines for the prototype micropump design. The MFSM micropump design can be readily adapted with the help of computational simulation to accommodate any further modifications.

In chapter 3, the fabrication process for MFSM micropump is discussed based on the prototype computational design. The fabrication process follows the order of importance for the

MFSM module such as diaphragm, micropump design, and assembly. The main materials comprising the module are polydimethylsiloxane (PDMS) and glass for micropump, channels, and the substrate. Fabrication of a novel diaphragm comprising of a PDMS/Ni-particle composite material is described. In chapter 4, the experimental setup is described and measurements made on the assembled fabricated layer are described. Experiments are performed with the prototype MFSM micropump module and the results are described.

Chapter 5 gives summary and conclusions of the research, and suggests future work on MFSM micropump modules. The latter includes: 1) design and fabrication of a solenoid and polymethyl methacrylate (PMMA) micropump chip and 2) development of a bonding method between PDMS and PMMA. These suggestions for further study will improve the MFSM micropump performance for obtaining more powerful devices for LOC, μTAS, and POCT.

CHAPTER 2

THE DESIGN OF MULTI-FLUIDIC SPEED-MODULATING (MFSM) MICROPUMP BASED ON SIMULATION RESULTS

Multi-fluidic speed-modulating (MFSM) micropump module is proposed here to overcome the current microfluidic chip issues such as cell agglomeration; and cost, size and convenience limitations resulting from the use of a conventional pump. MFSM micropump is an effective solution for lab-on-a-chip (LOC) device offering many benefits due to its small scale, ease of fabrications, and its ability to provide high performance controllable hydrodynamic focusing. The modulation of channel width and position due to hydrodynamic focusing is controlled by limiting the individual micropump flow rates. The designed micropump controls the diaphragm displacement against the main actuation force by interference between a permanent magnet and the PDMS/Ni-particle composite (PNPC) diaphragm.

The MFSM micropump module makes hydrodynamic focusing method possible with one small stack. In the design, the module size is overall 30 mm in length, 35 mm in width, and 15 mm in height as shown in Fig. 2.1 (b). One stack of the module is composed of three micropumps, and by modulating the pumping speed of each diaphragm makes it possible to control hydro-focusing of the fluidic channel. Despite the number of micropumps, the individual pump feature size is much smaller (several mm in length and width) than a typical syringe pump. In addition, MFSM micropump uses a simple energy source compared to some other micropumps. The MFSM micropump can also be manually operated by an external air pressure of a hand pump. The MFSM micropump is highly portable and readily adjustable to suit many applications because of its size.

The ultimate purpose of this project is to enable practical application of a microfluidic stack that integrates nanotechnology and microfluidics for biological applications as shown in Fig. 2.1 (a). This thesis covers aspects related to building a prototype design for modulating fluidic channel width and path by utilizing a hydrodynamic focusing method. The MFSM micropump for a fluidic transporting system developed here is a critical component of the complete system.

MFSM micropump utilizes reciprocation as a pumping mechanism with a functionalized diaphragm containing submicron nickel particles. The diaphragm of the MFSM micropump is pneumatically oscillated with pressure. The interaction between the PNPC diaphragm and the magnetic force resulting from a permanent magnet located above the diaphragm helps to control the pumping performance by varying the diaphragm displacement.

The MFSM micropump is composed of three main elements as shown in Fig. 2.1 (b). These are 1) the chamber and the valve layer, 2) PNPC diaphragm, and 3) the driving and modulating layer. The conceptual view in Fig. 2.1 (c) illustrates how the MFSM micropump module can be connected and assembled to form the complete microfluidic stack for supplying sample fluid, conveniently and more efficiently compared to a conventional pump.

Figure 2.2 illustrates the mechanism of channel modulation utilizing the hydrodynamic focusing method by controlling interference between a permanent magnet and the functionalized diaphragm. The presence of a magnet above the PNPC diaphragm controls the displacement of the diaphragm underneath and hence reduces the diaphragm stroke volume resulting in a reduction of the flow rate.

Chamber and valve layer provides the path for the fluidic flow. This layer has a chamber and two valves (inlet and outlet). When PDMS/Ni-particle composite diaphragm is made

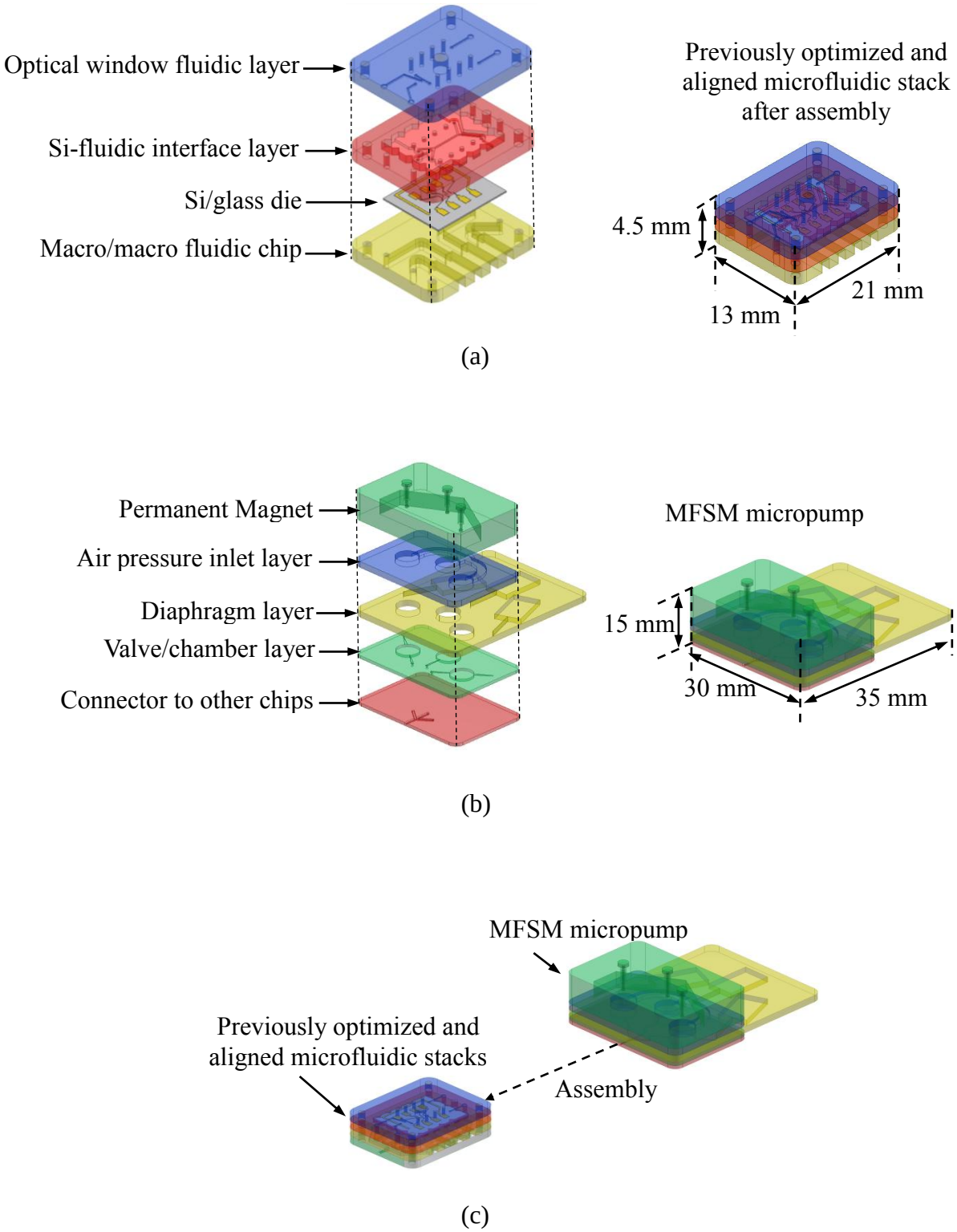

Fig. 2.1 (a) A modular microfluidic stack, after reference [17], (b) the initial concept of the MFSM micropump proposed in this work, and (c) system assembly.

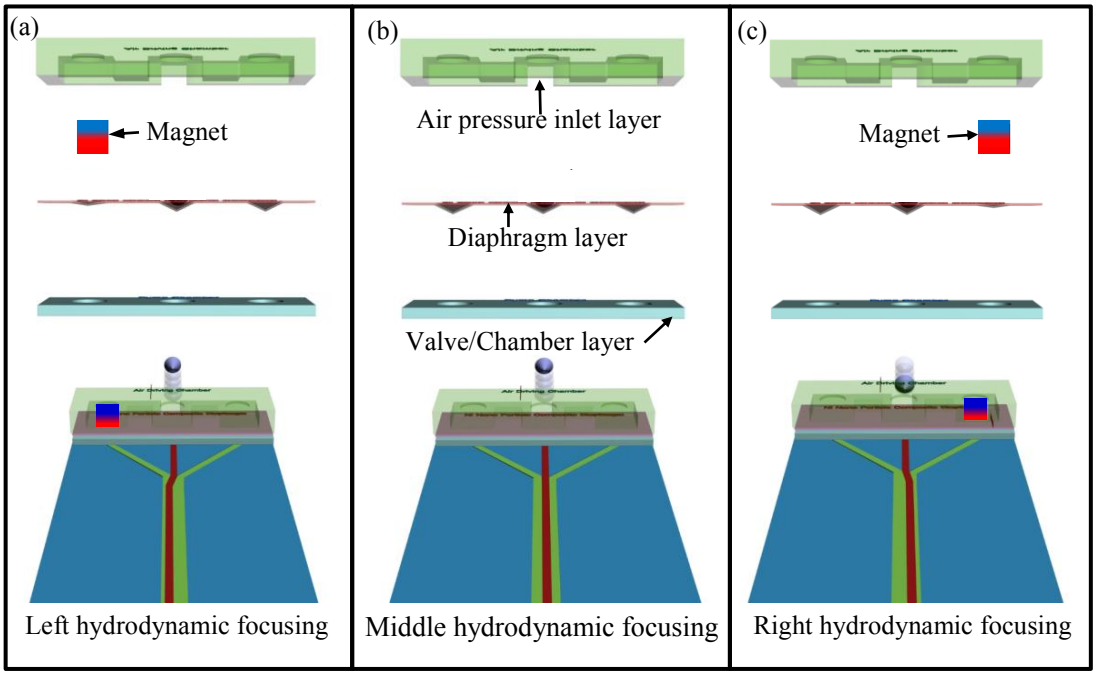

Fig. 2.2 Channel modulation with hydrodynamic focusing method utilizing a permanent magnet.

to oscillate by the external pressure at a certain frequency, the fluid is pushed out of the chamber due to reduction in the chamber volume and the fluid is drawn into the chamber by increasing the chamber volume. Fixed inlet and outlet valves have no moving parts, and the shapes of the valves determine the direction of the fluid flow.

PNPC diaphragm is a key part of the reciprocating pump. The diaphragm is made from a mixture of polydimethylsiloxane (PDMS) and nickel submicron particles. The diaphragm can be operated by an external force without submicron nickel particles. Nickel particles functionalize the diaphragm with respect to a magnetic force. Nickel particles decrease the displacement of the diaphragm due to magnetic interference from a permanent magnet present on the top layer.

Driving and modulation layer applies the external driving force for operation and the magnetic force for modulation. External pressure creates diaphragm displacement and can make the diaphragm to oscillate for pumping. For pumping speed modulation, permanent magnet

located in the middle of the layer approaches close to the diaphragm. Magnetic force influences the submicron nickel particle composite diaphragm by pulling the diaphragm up. Thus, two different forces in the opposite direction make it possible to control the amount of diaphragm deflection.

2.1 Diaphragm Simulation

Diaphragm is a key part of MFSM micropump which utilizes diaphragm reciprocation. The flow rate depends on the stroke volume, which is the volume change of the chamber caused by diaphragm motion. In reciprocating method, the stroke volume variation is entirely dependent upon the diaphragm displacement. This means that a larger diaphragm displacement creates larger stroke volume. Thus, calculation of the diaphragm displacement is important for predicting flow rate and working performance.

A specific diaphragm shape whether square, rectangular, or circular should be decided before the simulation. Circular diaphragm shows better displacement for the same external force compared to a square or a rectangular diaphragm, since the latter shapes suffer from high stress values at the corners. Thus, circular diaphragm was adapted in this displacement simulation [15]. In the diaphragm design, submicron nickel particles are implanted or mixed with PDMS to make the functionalized diaphragm. The simulation shows the deflection resulting from the external force. The effect on the nickel particles on the PDMS material properties is neglected in the simulation. Figure 2.3 shows the PDMS diaphragm with diaphragm radius (a) where uniform pressure (q) is placed over a circular area of radius (c) which is the radius of the particle loaded area along r-axis. The diaphragm displacement (w) toward w-axis by pressure can be calculated by the following equation [15]:

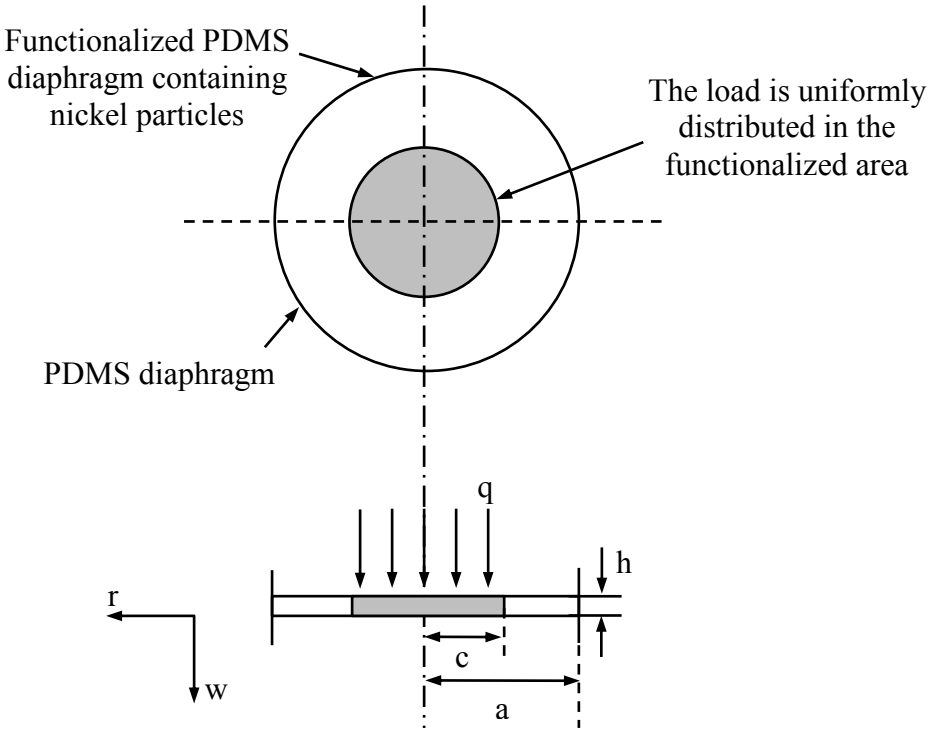

Fig. 2.3 The schematic of the object loaded diaphragm. After reference [29].

$$w(r) = \frac{qc^2}{8D}[(\log_e(\frac{1}{k}) - \frac{1}{4k^2})r^2 + \frac{c^2}{2}\log_e(\frac{1}{k}) - \frac{3c^2}{8} + \frac{a^2}{2}], \tag{2.1}$$

where k = a/c. For the diaphragm flexural rigidity expressed as $D = Eh^3/12(1-v^2)$, where E is Young's modulus, h is the diaphragm thickness, and v denotes the Poisson's ratio [29]. The maximum diaphragm displacement w_{max} can be obtained for r = 0 at the center as

$$w_{max} = (\frac{Fc^2}{16\pi D}) \cdot (k^2 - \log_e(k) - \frac{3}{4}), \tag{2.2}$$

where $F = \pi c^2 q$ is the total force acting on the diaphragm. Diaphragm is uniformly loaded when k = 1. This corresponds to the case when the nickel particles are uniformly distributed in the diaphragm as is the case in this work. For the case with k = 1, $w_{max} = Fa^2/64\pi D$ is the value obtained for maximum diaphragm displacement at the center r = 0.

Since the diaphragm is symmetrically deflected, simulation results are carried out over diaphragm. Simulation results vary depending on the diaphragm design parameters such as material, diameter, loaded length, thickness, and the magnitude of externally applied pressure. In this simulation, the implanted particle radius c is equal to the entire PDMS diaphragm radius a = 2.5 mm (i.e. k =1) with thickness h = 100 μm. The applied force value was 0.5 mN to PDMS diaphragm with respectively Young's modulus 350 kPa and Poisson's ratio 0.5. The maximum resulting deflection w_{max} at the center was 388 μm.

2.2 Magnetic Simulation

MFSM micropump can realize hydrodynamic focusing by interaction of a magnetic field with the PDMS/Ni-particle composite diaphragm. This interaction between the magnetic field and the functionalized nickel composite diaphragm controls the diaphragm displacement. A cylindrical permanent magnet 1 mm in height and 2 mm in diameter was used in these simulations utilizing COMSOL. The central position of the magnet is located at the origin in Fig. 2.4. These simulations showed that the magnetic field as expected, gradually decreases with distance from the magnet as shown in Fig. 2.4.

As shown in Fig. 2.5 (a), the magnet is located above the PDMS/Ni-particle composite diaphragm with 5 mm distance between magnet and PNPC diaphragm. Magnetic field on the PNPC diaphragm is affected by distance, so net magnetic force on the diaphragm with a certain distance was calculated utilizing MATLAB as shown in Fig. 2.5 (b). The force is inversely proportional to the distance between permanent magnet and the PDMS/Ni-particle composite diaphragm whose permeability is assumed to be high.

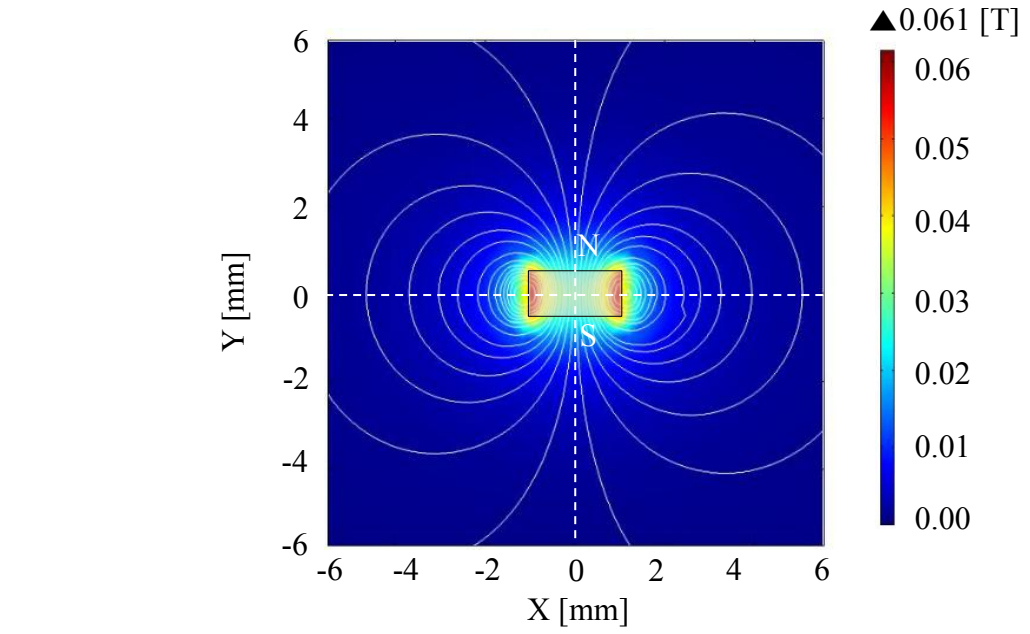

(a)

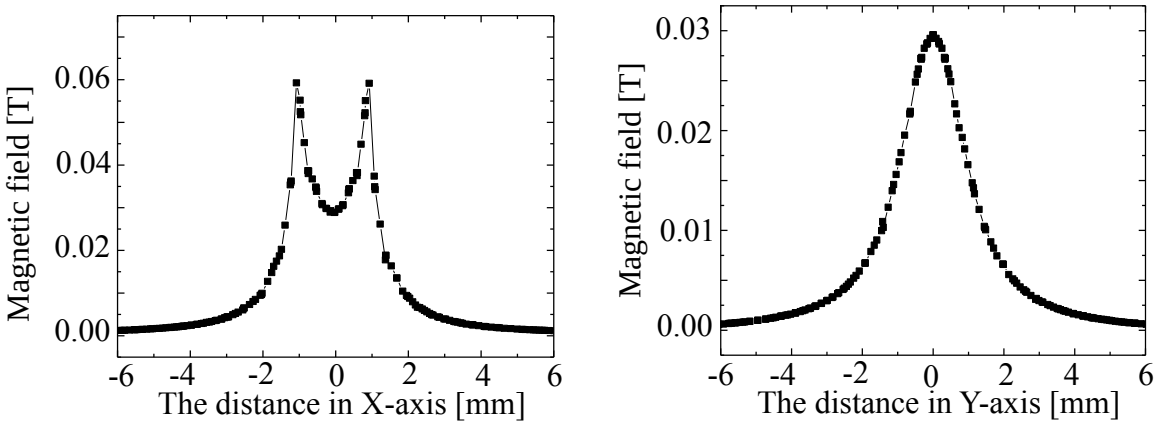

(b) (c)

Fig 2.4 Permanent magnet (2 mm dia x 1 mm height) and its magnetic field. (a) Magnetic field (2-D simulation), (b) magnetic field along the X-axis, and (c) magnetic field along the Y-axis.

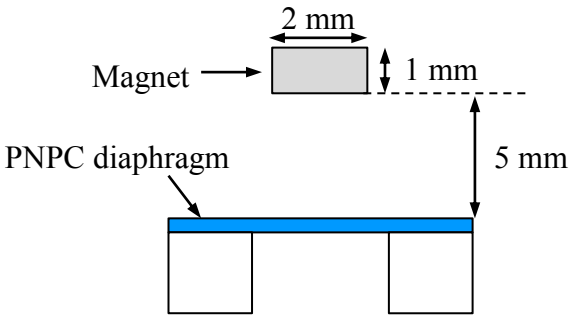

(a)

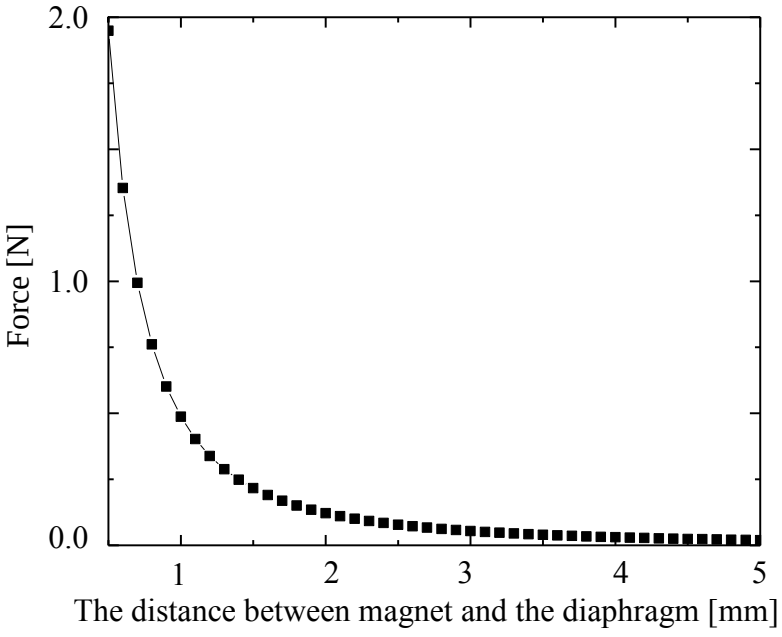

(b)

Fig. 2.5 (a) The magnet and PNPC diaphragm positions for magnetic net force. (b) Net force on the diaphragm of 5 mm diameter as a function of distance due to the permanent magnet. The distance is measured along y-direction in Fig. 2.4.

2.3 Micropump Flow Rate

In this section, micropump flow rate has been calculated to design a single micropump for the MFSM module. Flow rate calculation provides two benefits. First, the single micropump design based on calculation can provide certain general design guidelines for the MFSM micropumps. Second, it offers convenience in adjusting the design to address changes in fabrication, material system, specific flow rate, etc.

Many micropumps have been designed for microfluidics research. Micropump with static and fixed geometry valve has been attractive as a BioMEMS component due to its fabrication simplicity and good performance. Nozzle-diffuser and Tesla-type valves are two common types of static and fixed geometry passive valves. However, a Tesla-type valve is difficult to simulate because of its structural complexity. In this section, the flow rate is calculated for the nozzle-diffuser case.

Figure 2.6 shows that the fluidic flows from left to right under diaphragm motion as a result of the supply and the pump mode actions. During the supply mode, fluid is sucked into the chamber from both the nozzle and the diffuser ends, but fluidic flow rates in two cases are different because of the difference in the pressure drop at either end due to the geometrical shape. During the pump mode, the fluid flows out of the chamber through both the nozzle and diffuser ends, but the amount of fluid coming out due to the diffuser action is larger than due to the nozzle action. Thus, the majority of the fluid will flow toward one direction in spite of minor back flow which is a disadvantage for static and fixed geometry passive valve structures.

The calculation can be divided into two parts corresponding to the nozzle and the diffuser sides as indicated in Table 2.1. Each part of the nozzle and diffuser is considered at very low Reynolds numbers ($1 < R_e < 50$). ξ_n and ξ_d are respectively the total pressure loss coefficients at

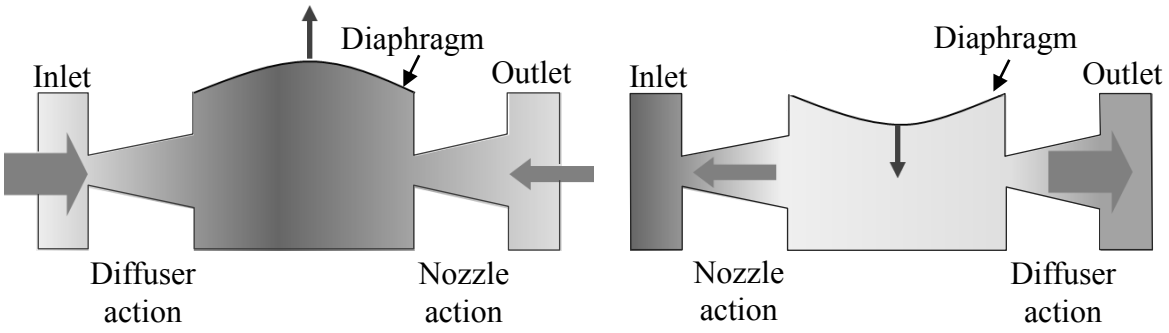

(a) (b)

Fig. 2.6 Conventional pump operation with a nozzle-diffuser structure. (a) Supply mode and (b) pump mode.

the nozzle and the diffuser ends and α is nozzle-diffuser angle (< 40°). n_o is the area ratio of D_0 over D_1 which defines as the smaller and larger diameter of the nozzle-diffuser shape [30]. The calculation considers geometric factor (A_n and A_d) and Reynolds number (Re) to determine the nozzle-diffuser performance.

The micropump flow rate (Q) with nozzle-diffuser configuration can be obtained from:

$$Q = \frac{2\Delta V_m \sqrt{\xi_n / \xi_d} - 1}{T\sqrt{\xi_n / \xi_d} + 1}. \tag{2.3}$$

The volume change (ΔV_m) of the diaphragm with actuation period (T) is given by

$$\Delta V_m = \frac{Fa^4}{192D}, \tag{2.4}$$

Table 2.1 Nozzle-diffuser equations for low Reynolds number. After reference [30].

Nozzle flow	Diffuser flow
$\xi_n = \frac{A_n}{\mathrm{Re}}$ $A_n = \frac{19}{n_0^{0.5}(\tan\alpha)^{0.75}}$	$\xi_d = \frac{A_d}{\mathrm{Re}}$ $A_d = \frac{20(1/n_o^2)^{0.33}}{(\tan\alpha)^{0.75}}$

where, F, a, and D are respectively the total load acting on the diaphragm (0.3 mN), diaphragm radius (2 mm), and flexural rigidity (E = 350 kPa, ν = 0.5, and h = 100 μm) of the diaphragm. The nozzle-diffuser with small conical angle shows better result for the low Reynolds number [30]. D_0 in $A_{n,d}$ calculations is 100 μm with an angle in the range $4^{\circ} < \alpha < 40^{\circ}$. It is assumed that the working fluid is water with Re = 5 with applied flow velocity 0.05 mm/s for $\xi_{n,d}$ calculations. From equation 2.3, the flow rate (Q = 0.104 ml/min) can be achieved as a function of flow coefficient ratio (ξ_n / ξ_d = 3). The latter depend on geometric factors such as diameter ratio, conical angle, the area ratio of the inlet/outlet and the Reynolds number.

The flow rate calculation of the micropump was performed only with nozzle-diffuser configuration due to the lack of equations for Tesla-type valve. However, the performances of nozzle-diffuser and Tesla-type valve in practical design structures are comparable from the experimental results [28]. Table 2.2 compares diodicity of these two valve configurations. Based on Table 2.2, Tesla-type valve generally has better performance than the nozzle-diffuser structure. Thus, Tesla-type valve will be fabricated for the prototype MFSM micorpump design in this work instead of the nozzle-diffuser design, since Tesla-type valve generally shows better performance than the nozzle-diffuser structure. The Tesla-type valve simulations have been carried out by the computational fluidic dynamics (CFD) simulation tool in ANSYS.

Table 2.2 Diodicity vs. Reynolds number comparison between nozzle-diffuser and Tesla-type valve. After reference [28].

Nozzle-diffuser				
Reynolds number	250	350	500	700
Diodicity	1.3	1.4	1.7	1.75
Tesla-type valve				
Diodicity	1.6	1.7	1.8	1.9

The Tesla-type valve structure with 150 μm × 150 μm in channel width and height respectively is shown in Fig. 2.7 (a). In order to get diodicity of the valve, inlet flow is applied into forward and reverse directions, and the pressures in inlet and outlet are compared. When water flow through this geometry is 0.1 ml/min having Reynolds number of 11.26, the simulation results indicate diodicity to be 1.058 as indicated in Fig. 2.7 (b).

2.4 Prototype Design of Multi-Fluidic Speed-Modulating (MFSM) Micropump

The fabrication process follows the schematic illustrated in Fig. 2.8. Figure 2.8 (a) illustrates the overall oblique view of the prototype modulation module. The cross-sectional view is shown in Fig. 2.8 (b) and the plan view of MFSM micropump channel layer is shown in Fig. 2.8 (c). The top and bottom PDMS layers contain the mold design of the MFSM micropump, the air pressure inlet and the magnets. Bolt and nut assembly for manipulating the magnetic force are incorporated during the casting process of the top PDMS layer. The middle layer is PDMS diaphragm which contains nickel particles. The layers are built on a glass substrate, and the device dimensions for the top PDMS layer are: 20 mm width, 30 mm length, and 15 mm thickness. According to the micropump calculation results of a nozzle-diffuser valve, the expected flow rate of the each micropump is about 100 μm/min, but the prototype design uses Tesla-type valve, whose performance is better than the nozzle-diffuser structure. Thus, the measured flow rate is expected to be higher than the values obtained from the nozzle-diffuser simulation.

	Tesla-type valve
Forward	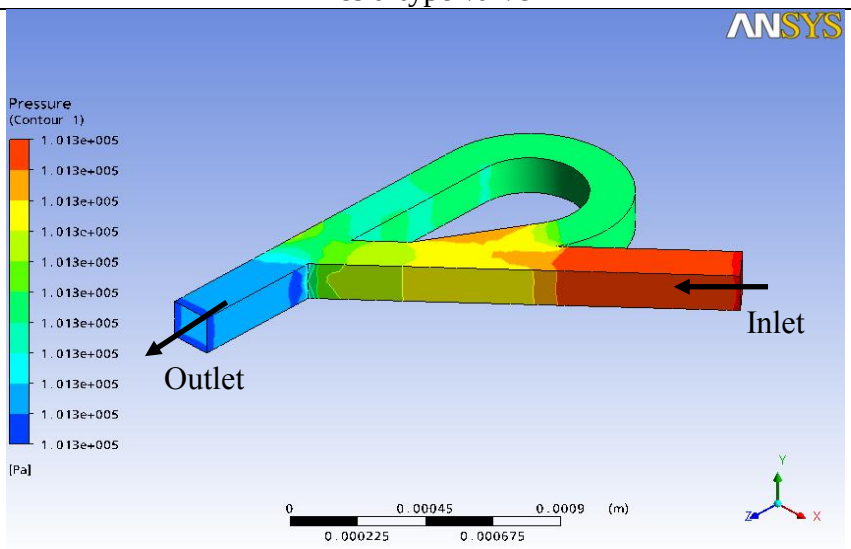
Reverse	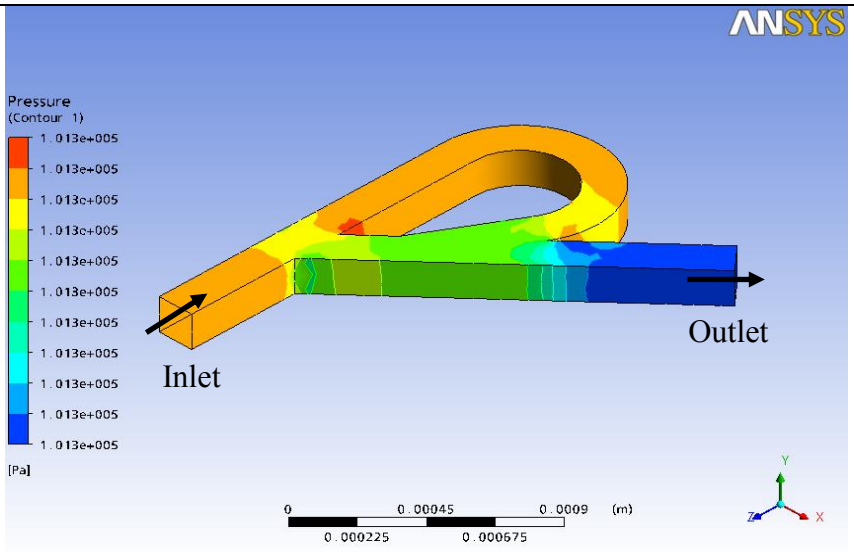

(a)

	Flow direction	Point	Pressure [Pa]	ΔP [Pa]	Diodicity (D_i)
Tesla-type valve	Forward	Inlet	101342	17	1.058
		Outlet	101325		
	Reverse	Inlet	101343	18	
		Outlet	101325		

(b)

Fig 2.7 Tesla-type valve (a) simulation and (b) diodicity.

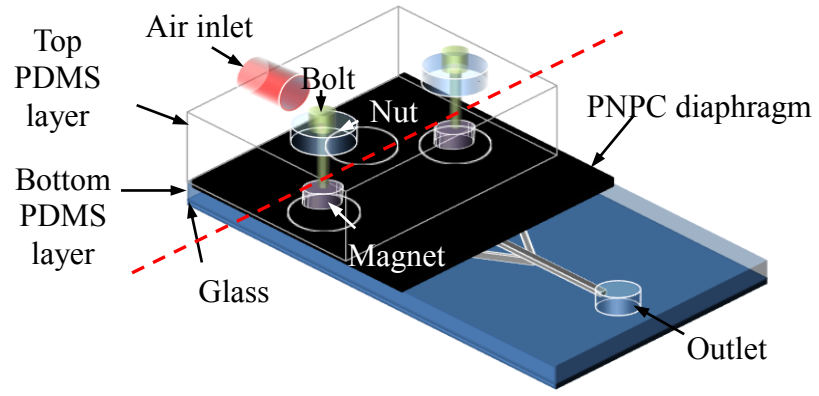

(a) Oblique view

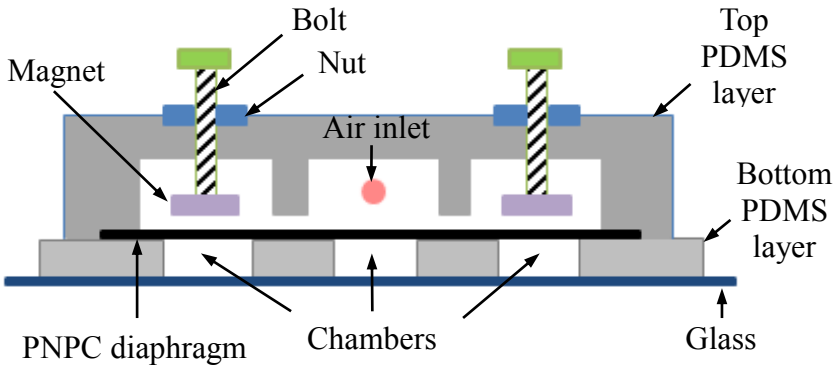

(b) Front cross-sectional view

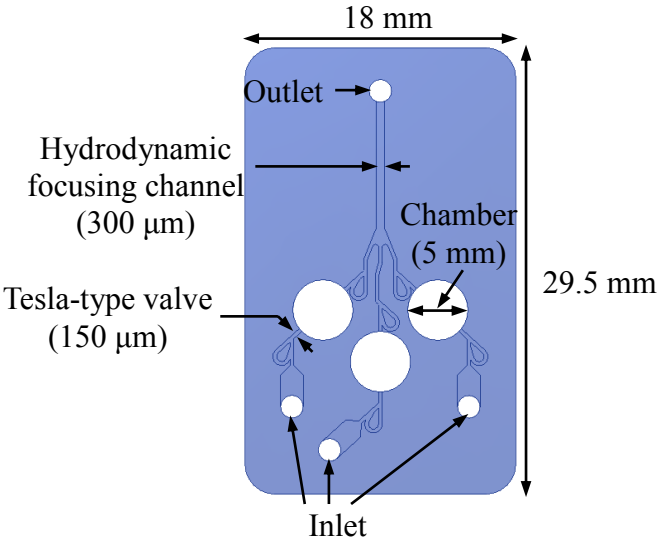

(c) Plan view of channles in the bottom PDMS layer

Fig. 2.8 MFSM micropump drawing and schematic with (a) oblique view, (b) front cross-sectional view, and (c) plan view of channels in the bottom PDMS layer.

CHAPTER 3

THE FABRICATION OF MULTI-FLUIDIC SPEED-MODULATING (MFSM) MICROPUMP BASED ON THE DESIGN

The initial prototype design of the multi-fluidic speed-modulating (MFSM) micropump is based on the simulation results. The fabrication sequence is then determined for the prototype design. This chapter describes the method for the device fabrication. The fabrication can be divided into three main processes: 1) diaphragm fabrication, 2) micropump molding step, and 3) bonding. More details will be explained in the sections given below.

3.1 PDMS/Ni-Particle Composite (PNPC) Diaphragm

PDMS/Ni-particle composite diaphragm is one of the key parts of the MFSM micropump module. A polymer diaphragm containing submicron nickel particles is fabricated to realize modulation of fluid flow in the MFSM micropump. Polydimethylsiloxane (PDMS) (Sylgard 184 Silicone Elastomer, Dow Corning Corporation) is used and mixed with 5:1 volume ratio of pre-polymer and cross-linker to obtain a compact matrix formation with submicron nickel particles [31]. Submicron 99.8 % nickel particles are purchased from (Sigma-Aldrich Corporation). Figure 3.1 shows scanning electron microscope (SEM, Hitachi S-4500 II) pictures of nickel particles. Submicron nickel particles comprising of 10, 20, and 40 by wt% are used in the PDMS mixture with pre-polymer and cross-linker. The nickel particles are hence incorporated into the matrix of the polymer.

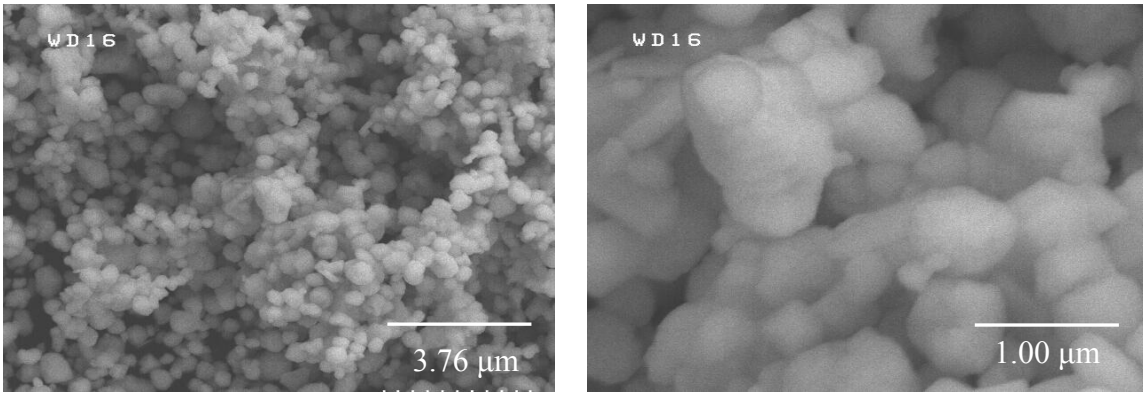

Fig. 3.1 Scanning electron microscope (SEM) images of the submicron nickel particles.

However, submicron nickel particles have an agglomeration problem similar to other nanometer and micrometer sized particles. Hence, a solvent, toluene (Toluene anhydrous, 99.8 % from Sigma-Aldrich Corporation), is used to prevent agglomeration of particles [31]. Sonication of the particles with toluene is carried out for 30 minutes to effectively disperse the particles. The pre-polymer is then added to the prepared toluene solution with particles. The mixture of nickel particle, toluene and pre-polymer is stirred uniformly and then put into the sonication bath for 30 minutes. The composite solution is placed under a fume hood to allow toluene to evaporate for 24 hours. After the prepared solution is ready, the fabrication procedure is outlined in Fig. 3.2. To solidify the polymer, PDMS cross-linker is added and mixed thoroughly for 10 minutes and then degassed in a vacuum chamber for 30 minutes. Nickel particle implanted polymer diaphragm is fabricated by spin coating on an intermediate kapton film. Thin polymer diaphragm is typically difficult to detach from silicon substrate, so the kapton film makes the composite film easy to detach from the silicon substrate.

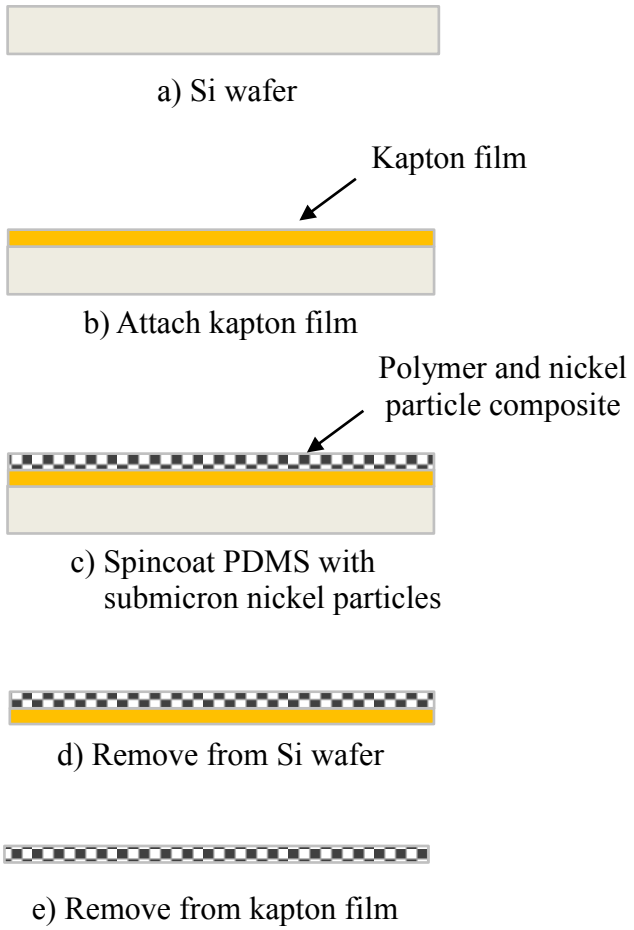

Fig. 3.2 PDMS/Ni-particle composite (PNPC) diaphragm fabrication procedure.

The fabricated PNPC diaphragm is shown on Fig. 3.3. The diaphragm which contains 20 wt% of the submicron nickel particles has no visible agglomeration on the surface. However, the diaphragm which contains 40 wt% of the submicron nickel particles shows agglomeration. This is an obstacle in controlling the diaphragm thickness. Hence, in this work the nickel particles wt% in the pre-polymer mix did not exceed 20 wt% to avoid particle agglomeration.

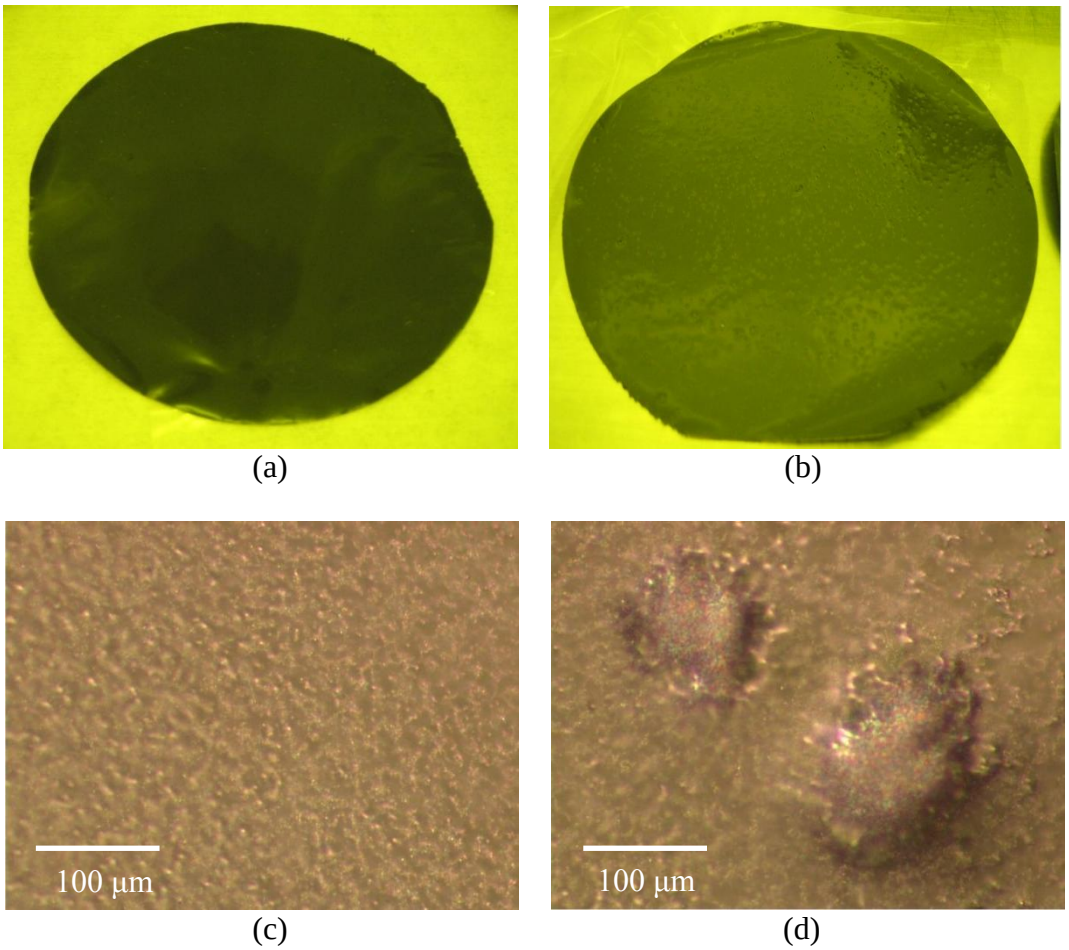

Fig. 3.3 PNPC diaphragms (a) with 20 wt% and (b) with 40 wt% of nickel particles. Microscope views of (c) 20 wt% and (d) 40 wt% nickel composition cases. Note particle agglomeration in (d).

3.2 Mold Design

The MFSM micropump design obtained in this work is shown in Fig. 3.4 and is drawn with AutoCAD. The design is based on simulation results described in chapter 2. Several possible designs have been considered by varying the chamber size and the channel width to meet the flow rate requirement. The hydrodynamic focusing channel length is kept at 9 mm for all designs as shown in Fig. 3.4. Individual micropumps are also designed for test purposes and are located at both sides of the mold. Initially, a simple nozzle-diffuser was used in the simulation as a static and fixed geometry valve. According to the literature study, a Tesla-type valve gives better performance compared to a nozzle-diffuser design. As a result, a Tesla-type valve is the one used here in the prototype module design. This made the designed chip size slightly larger than the standard fluidic stack chip that CAMD had proposed initially.

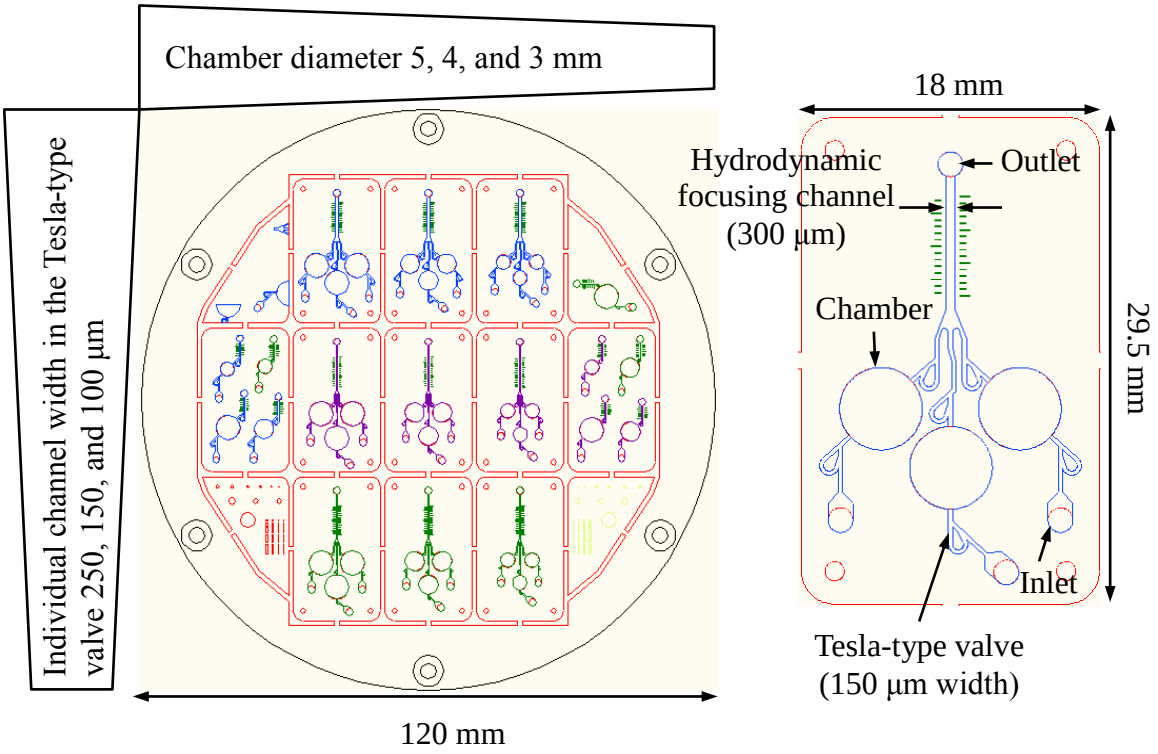

Fig. 3.4 MFSM micropump designs with varying channel width and chamber diameter values.

3.3 Mold Fabrication

Precision micromilling machine (Kern Precision, Inc.) is employed to fabricate a brass mold insert as per design specifications. Though this process of fabricating a mold insert is well-suited for rapid prototyping, the use of a milling tool that has size limitations also limits the quality of some structure details. If a 500 μm deep structure needs to be milled, a milling bit no longer than 200 μm diameter is required to realize the designed structure. Thus, some structures in the graphical design in Fig. 3.4 will not always have exactly the same features as intended in the mold insert design.

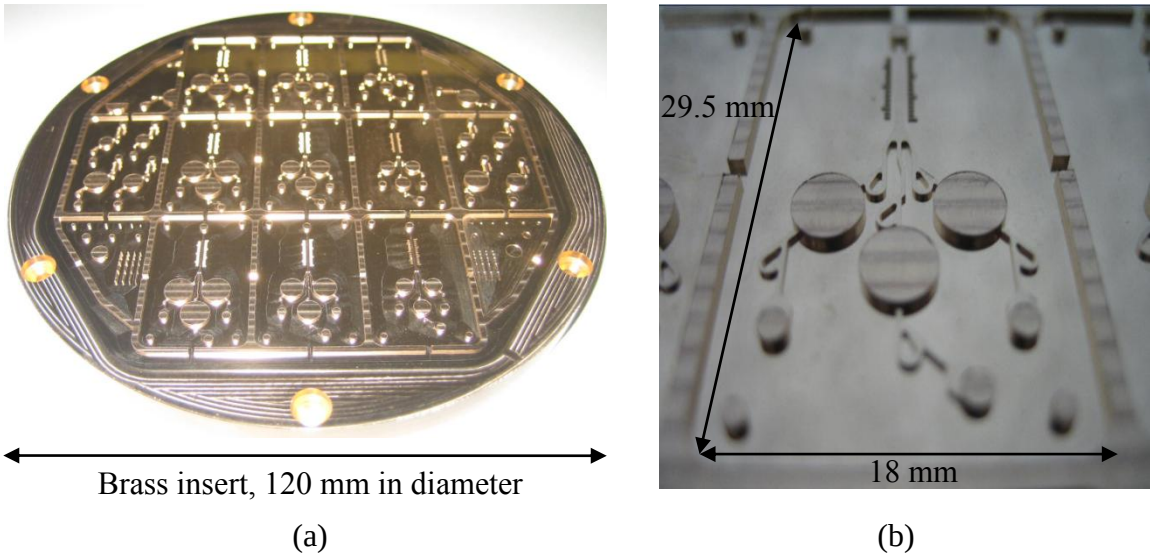

Fig. 3.5 (a) MFSM micropump brass mold obtained by micro-milling. (b) Zoomed in view of details on a chip area.

3.4 Tesla-Type Valve Fabrication

MFSM micropump makes use of a static and fixed geometry valve due to its reliability and simplicity of fabrication. Nozzle-diffuser and Tesla-type valve are two main examples of static and fixed geometry valves. For MFSM micropump, the Tesla-type valve has been adapted because of its superior rectification.

An “optimum” design of the Tesla-type valve has been described by Adrian R. Gamboa *et. al* [27] and is shown in Fig. 3.6 (a). But this “optimum” design obtained using AutoCad could not be realized in the fabrication of the brass mold insert because of the limitations on the strength of the milling bit of the milling machine. The actual shape obtained on the mold insert shown in Fig. 3.6 (b) is somewhat different from the designed shape, because the available milling machine required a minimum of 200 μm diameter milling bit in order to cut a structure with 500 μm depth for the milling bit not to be damaged. Hence, the sharp edges on the optimum Tesla-type design appear to be slightly round due to the large diameter of the milling bit employed.

Simulation results have been carried out using ANSYS for the two design shapes corresponding to before and after milling machine operation and are shown in Fig. 3.7. The expected fluidic flow rate in the pump simulation is 0.1 ml/min. This volume of the flow can be achieved by applying 74.07 mm/s fluidic velocities in both forward and reverse directions for 150 μm channel width used in computational simulation. The Tesla-type valve is able to achieve

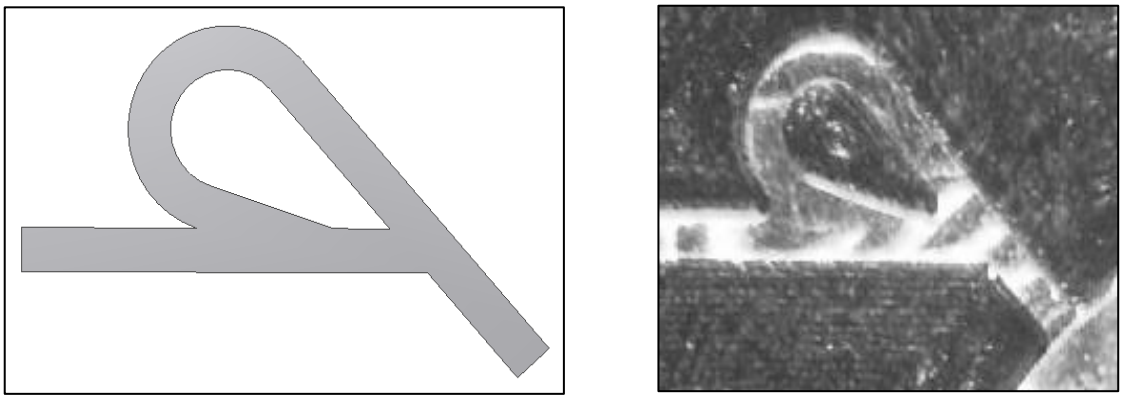

(a) (b)

Fig. 3.6 The milling machine limitation effect on the structures. (a) The optimum design shape of the Tesla-type valve, after reference [27] and (b) the Tesla-type valve obtained with the milling machine used.

11.26 Reynolds number. The diodicity, defined as the rectification ratio, is compared for the two shapes in Table 3.1. The changed design shape as a result of the milling machine limitation reduces rectifications than the original design with diodicity of 1.021 compared to 1.058 for the "optimal" design case. The round structure in Tesla-type valve results in smooth streams in forward and reverse flow and hence, it cannot rectify the stream efficiently.

	The "optimum" design	The changed design with milling machine
Forward direction	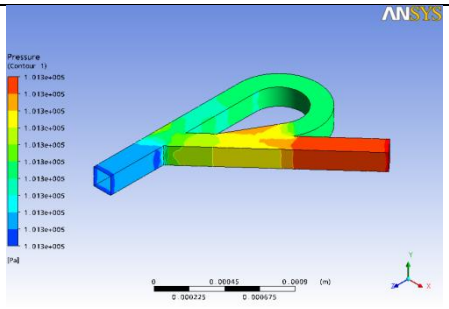	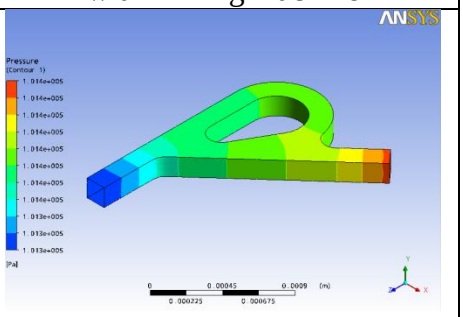
Reverse direction	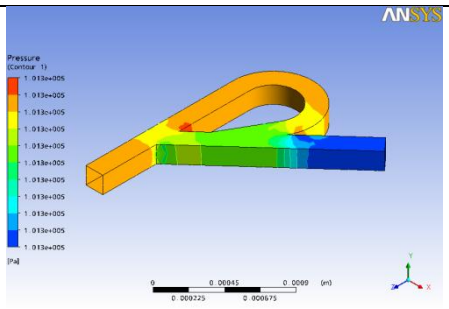	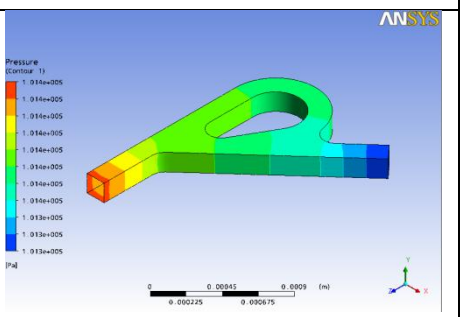

Fig. 3.7 Tesla-type valve fluidic simulation on ANSYS.

Table 3.1 Tesla-type valve diodicity simulation data based on the design shapes.

	Flow direction	point	Pressure [Pa]	ΔP [Pa]	Diodicity ($Di = \frac{\Delta P_{Reverse}}{\Delta P_{Forward}}$)
"Optimum" design	Forward	Inlet	101342	17	1.058
		Outlet	101325		
	Reverse	Inlet	101343	18	
		Outlet	101325		
Design after machining	Forward	Inlet	101420	95	1.021
		Outlet	101325		
	Reverse	Inlet	101423	97	
		Outlet	101326		

3.5 Bonding Process

3.5.1 Polydimethylsiloxane (PDMS) to Glass

One of the most common materials for biocompatible microfluidic devices is PDMS because of simplicity in fabrication, elasticity, and transparency. Another significant benefit of PDMS is the relative ease of bonding with other materials such as silicon wafer and glass by oxygen plasma treatment. In microfluidics, tight sealing is required because of the fluid phase of the material in microfluidic applications. Any microfluidic device using PDMS and glass slide can be made leak-free by a reliable bonding process called oxygen plasma bonding. The surface of the PDMS and glass can be modified by the oxygen plasma treatment. PDMS surface is composed of -O-Si$(CH_3)_2$- group. When the group is exposed to oxygen plasma, the silanol groups (-OH) combines with the methyl groups (-CH_3). These chemical reactions ultimately produce Si-O-Si covalent bond which sustains 30-50 psi bonding pressure [32].

Center for Advanced Microstructures and Devices (CAMD) at LSU has an O_2 plasma machine (Bransen Plasma Asher). It can generate a maximum of 1500 W rf power at 13.56 MHz. The bonding process in this work is performed at 150 W rf power at 450 mTorr pressure with 1 minute plasma exposure time. The layers are placed in the chamber for the treatment. After the treatment the layers are immediately brought in contact with each other outside of the chamber and pressed together with gentle pressure to achieve a bond.

CHAPTER 4

EXPERIMENT AND RESULTS

In this chapter, the experimental tests and the results are described. The PNPC composite diaphragm is first characterized by examining its displacement and mechanical properties. In addition, each layer of multi-fluidic speed-modulating (MFSM) micropump module is assembled and its performance for modulating channel width and achieving, hydrodynamic focusing are examined. At the end, the experimental results are discussed.

4.1 Diaphragm Characterization

For displacement measurements, a laser sensor or an optical microscope are typically used. In our case the optical microscope setup illustrated in Fig. 4.1 (a) is used. In the normal operation, pneumatic force for the diaphragm actuation is applied from above the diaphragm in the MFSM micropump, but the path of the force can block the optical measurement. Thus, an alternative jig was designed to apply pneumatic force for making displacement measurements as shown in Fig. 4.1. Fig. 4.2 shows the test structure that allowed the measurement of the diaphragm displacement by the microscope. The test jig for the diaphragm is made by casting polydimethylsiloxane (PDMS) that contains a channel, and the PDMS housing is bonded on the glass substrate by oxygen plasma treatment. Moreover, a needle is used as an inlet for applying pneumatic pressure to the test diaphragm. The latter is cut into proper size and bonded to the displacement test jig as indicated in Fig. 4.2. After the assembly, the final sealing is done by additional liquid PDMS to prevent any air leakage.

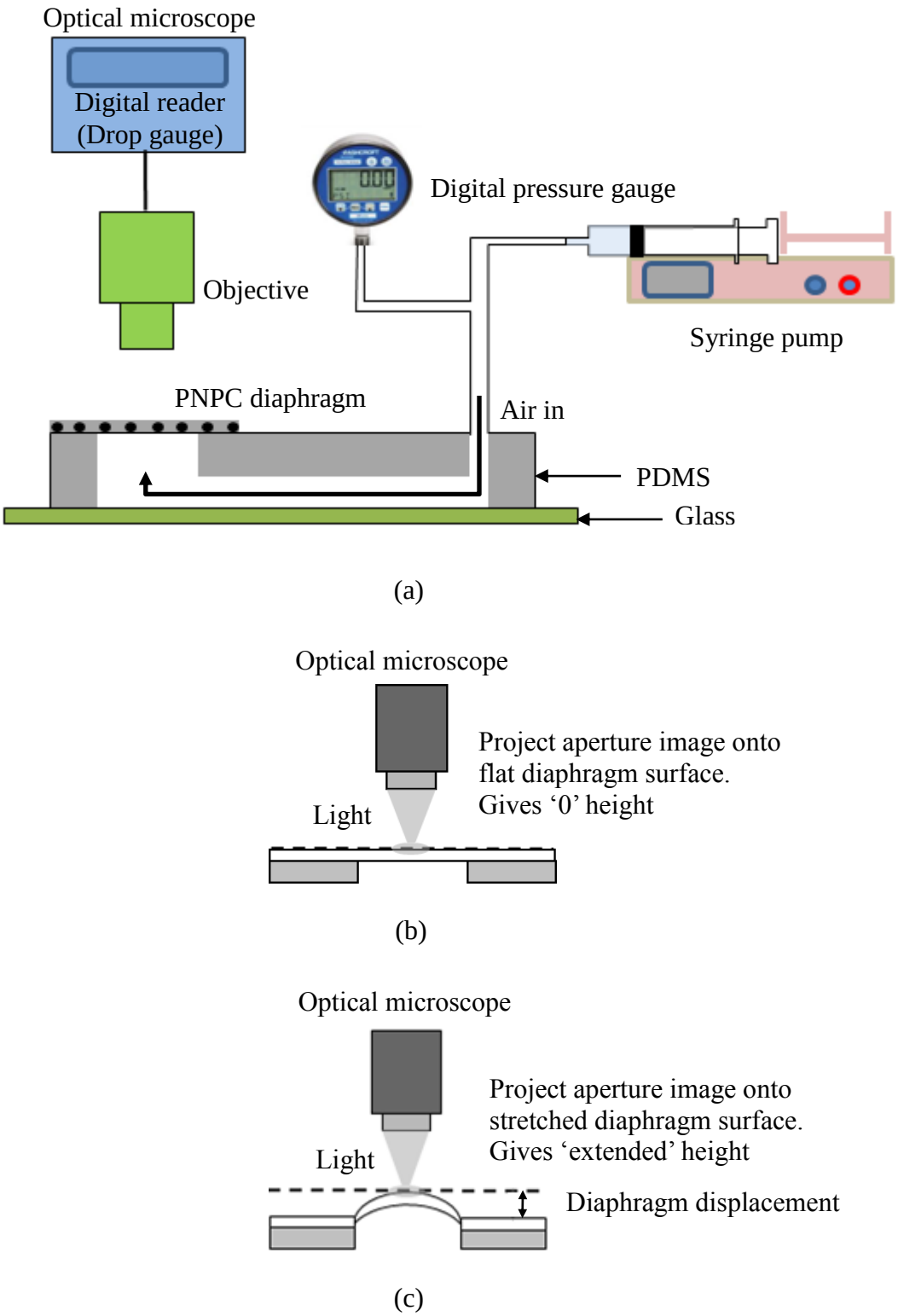

Fig. 4.1 (a) Schematic of the nickel particle implanted diaphragm displacement measurement setup. (b) Optical microscope focusing with no applied pressure and (c) optical microscope focusing with applied pressure.

4.1.1 Diaphragm Displacement Measurement

Diaphragm is commonly employed in a reciprocating pumping mechanism. Fluidic flow is achieved by the chamber volume change due to an oscillating diaphragm covering the chamber. Thus, diaphragm is one of the main components of the micropump. For PDMS/Ni-particle composite (PNPC) diaphragm displacement measurement, the optical microscope setup is illustrated in Fig 4.1 (a). First, the diaphragm is placed on the stage of the microscope and the aperture image is focused on the diaphragm surface as shown in Fig 4.1 (b). Second, the applied air pressure changes the height of the diaphragm, and the aperture image is refocused on the diaphragm surface as shown in Fig 4.1 (c).

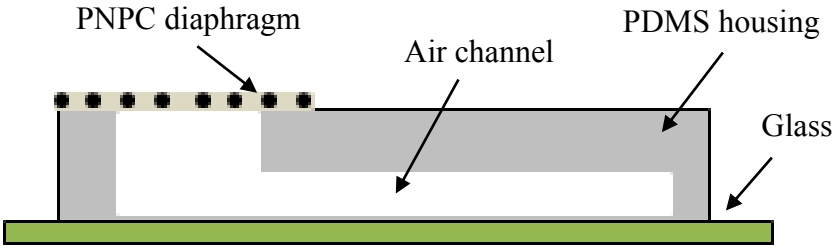

(a)

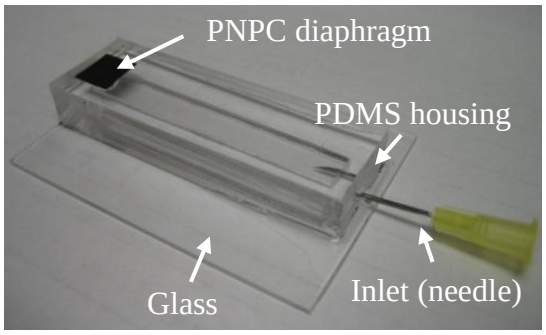

(b)

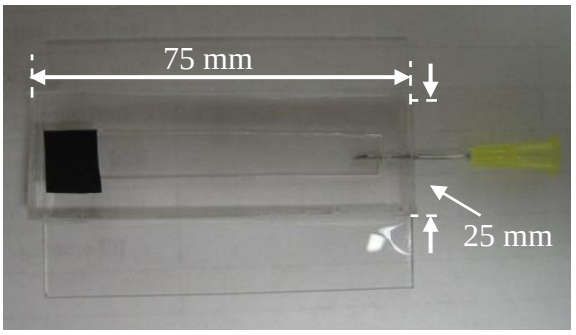

(c)

Fig 4.2 (a) The schematic of the test jig and its pictures in (b) oblique and (c) top view.

During the measurements, a syringe pump precisely controls the air pressure which is applied to the test jig. The pressure against the PNPC diaphragm is measured by a digital pressure gauge. The amount of deflection is measured by focusing the microscope onto the diaphragm surface and measuring the distance the microscope objective is moved to project a sharp image of the aperture onto the diaphragm surface. The distance traveled in the vertical z-direction is measured with a drop gauge attached to the microscope column. Displacement was measured several times, and the measurement error was about 4 μm due to human factors and equipment. The actual setup is shown in Fig. 4.3.

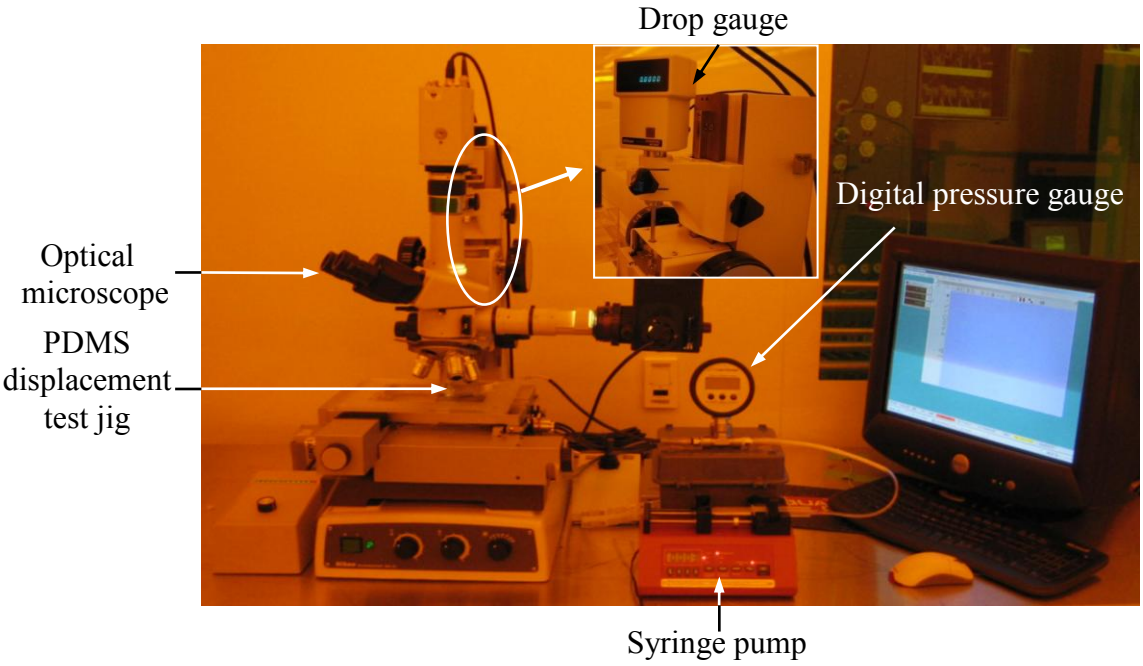

Fig. 4.3 The photograph of the measurement setup.

4.1.2 PDMS Diaphragm Measurement and Simulation Model

The micropump using reciprocation produces the pressure and flow rate which depend on many factors such as stroke volume, dead volume, frequency, valve characteristic, and fluid property. Among these factors, stroke volume and oscillating frequency are dominant for the pump performance. However, diaphragm properties restrict stroke volume and diaphragm displacement frequency. Therefore, diaphragm displacement calculation is important for determining more accurate flow rate of the micropump. Simulation results for diaphragm displacement are done using MATLAB based on the following equation [19]:

$$\frac{Pd^4}{16Et^4} = \frac{5.33}{(1-\nu^2)} \cdot \frac{y}{t} + \frac{2.6}{(1-\nu^2)} \cdot (\frac{y}{t})^3 . \qquad (4.1)$$

The diaphragm size and properties such as diaphragm diameter (d), thickness (t), Young's modulus (E), and Poisson ratio (ν) provide information to calculate the displacement (y) at the center of the diaphragm with applied pressure (P). A new simulation equation is introduced and compared with the previous simulation Eq. (2.1). These simulation results need to be confirmed by experiments using simple PDMS diaphragms. The results of experiments and simulations for a 120.6 μm thick PDMS diaphragm of diameter 5 mm are shown in Fig. 4.4. A circular opening underneath the PDMS/Ni-particle composite (PNPC) diaphragm shown in Fig. 4.2 a) gives the diaphragm diameter. The simulation Eq. (4.1) demonstrates a better agreement compared to Eq. (2.1) when the graphs from two equations are compared between the measured and the simulated data for a pressure range from 0.1 kPa to 4.0 kPa. Hence, use of simulation results for a PNPC diaphragm can be considered to be accurate. PDMS has a range of Young's modulus from 12 kPa to 2.5 MPa depending on the volume ratio between the pre-polymer and the cross-linker used [33]. From curve fitting procedure, Young's modulus of 2.3 MPa for the PDMS diaphragm gave the best fit to measured data with Possion's ratio of 0.5. This value seems to be

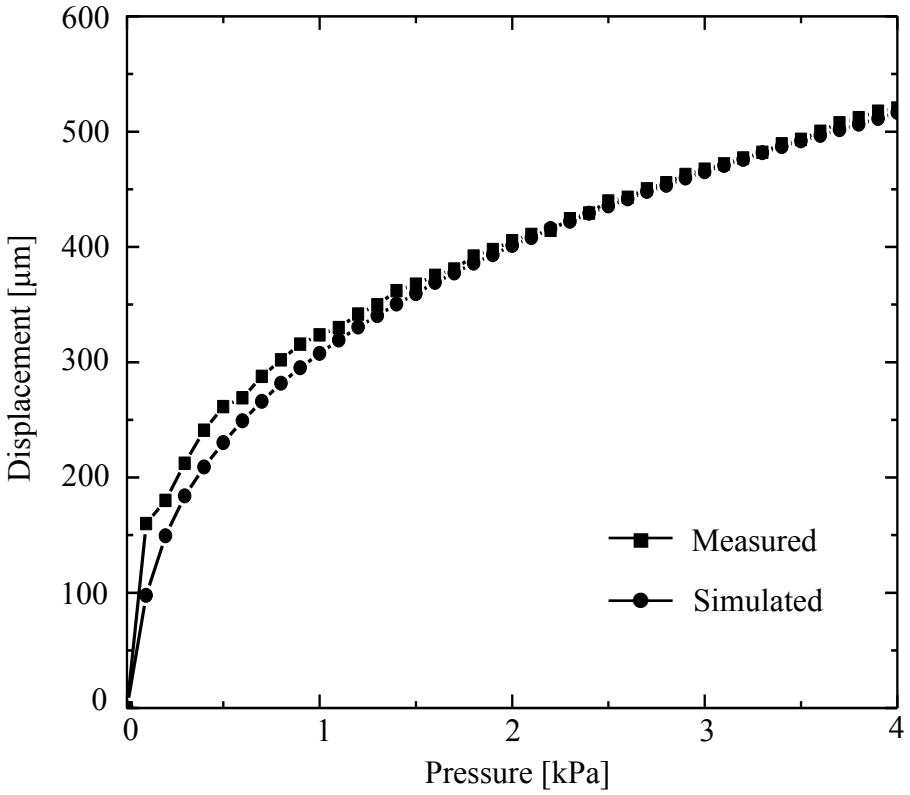

Fig. 4.4 The comparison of the measured and simulated PDMS diaphragm displacement.

a little high for the 1:5 volume ratio of cross-linker to pre-polymer used. However, the value is still in the accepted range of Young's modulus values for PDMS.

4.1.3 Displacement Measurement on PNPC Diaphragm

The displacement of the PDMS/Ni-particle composite (PNPC) diaphragm is measured with the method explained in section 4.1.1. The measurement was performed with a diaphragm containing 10 wt% of nickel particles in 90 wt% of cross-linker and pre-polymer. The weight percent of nickel in the diaphragm is arrived at using the following equations:

$$\alpha \cdot \mathrm{A} + \beta \cdot \mathrm{B} = M_{diaphragm\ mass} \tag{4.2}$$

$$\mathrm{A} + \mathrm{B} = V_{diaphragm\ volume}, \tag{4.3}$$

where α and β respectively represent density of nickel and PDMS and A is the volume of nickel and B is the volume of PDMS in the diaphragm. Here, α and β are 8.912 g/ml and 0.956 g/ml. $M_{diaphragm\ mass}$ is the mass of the fabricated diaphragm which is measured by a micro scale (AT460 DeltaRange, Mettler Toledo). $V_{diaphragm\ volume}$ is the volume of the diaphragm which can be calculated from the thickness and the area of diaphragm. From this, A and B can be calculated.

Table 4.1 shows the comparison between the initial weight of nickel particles used and the final values calculated from measurements on the diaphragm. The actual weight percent of nickel particles in 10 wt% nickel particle composite diaphragm is about 30 wt%, which is three times larger. The reason is the density difference arising between pouring of the liquid mixture before spincoat to the final solidified diaphragm due to loss of solvent. The Fig. 4.5 compares the measured diaphragm displacement with applied air pressure to the result obtained from simulation utilizing curve-fitted values for Young's modulus and Poisson's ratio of 1.55 MPa and 0.5 respectively for a diaphragm 170 μm thick and 5 mm in diameter. The simulation result lies between the measured values obtained for the two fabricated diaphragms given in Table 4.1.

Table 4.1 Weight percent comparisons obtained from initial ingredient used with the values measured on the fabricated diaphragms.

Sample number	Nickel [wt%]	Thickness [μm]	Mass [g]	Calculated nickel [wt%]	Young's modulus [MPa]
1	10	av. 172.8	0.297	29.74	1.60
2	10	av. 169.2	0.292	29.16	1.35

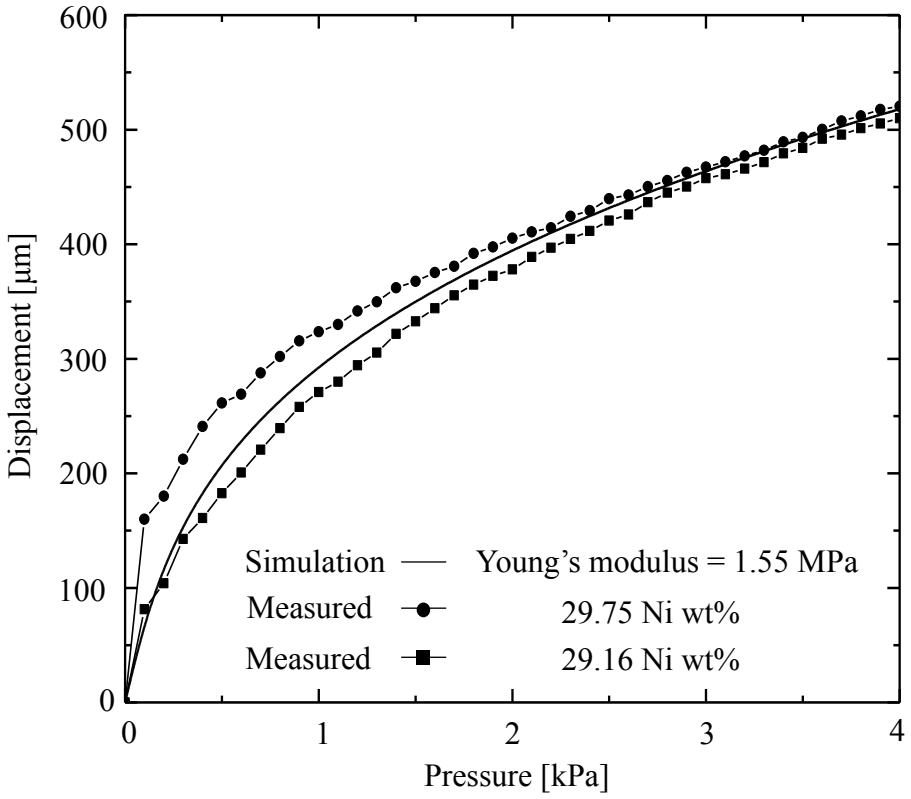

Fig. 4.5 The measured displacement of diaphragms formed from 29.74 wt% and 29.16 wt% PDMS/Ni-particle composite diaphragms.

4.1.4 Mechanical Property Measurement of PNPC Diaphragm

PNPC diaphragm is made from a mixture of PDMS and certain volume of nickel particles, hence, the diaphragm can show different mechanical properties such as hardness and elastic modulus depending on its composition. Indentation technique has been a primary method for determination of mechanical properties since 1992 and is quite attractive for high resolution measurements on micrometer and nanometer scaled structural features [34]. Hence, this technique was used to measure the mechanical properties of the diaphragm.

Figure 4.6 (a) shows the indentation (Triboindenter, Hysitron Cooperation) used. Figure 4.6 (b) shows the front view of the chamber which has a mounting stage and the measurement

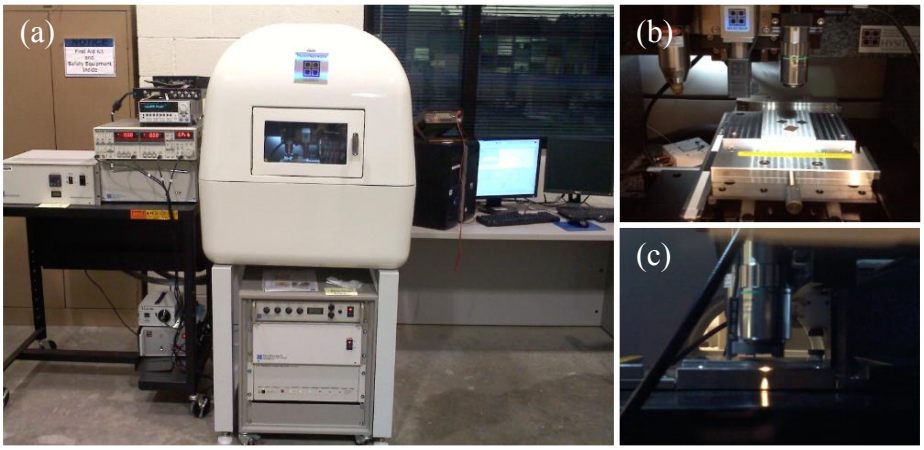

Fig. 4.6 Indentation measurement. (a) Indentation equipment setup, (b) front view, and (c) side view of the measurement stage, scope, and the loading tip.

tip. Figure 4.6 (c) is a picture taken during a mechanical test in process. Here, the tip is touching the sample diaphragm for the measurement.

The indentation measurements generate a graph from elasticity and hardness data obtained when the loading tip touches the PNPC diaphragm as indicated in Fig. 4.7. The measurement is conducted at four random points on the diaphragm and average of these measurements provides the values for the effective elasticity (E_r) and hardness (H). The average measured value for effective elasticity E_r is 3.76 MPa.

E_r, the effective elastic modulus which is expressed as

$$\frac{1}{E_r} = \frac{(1-\nu^2)}{E} + \frac{(1-\nu_i^2)}{E_i} \quad [35]. \tag{4.4}$$

E is Young's modulus and ν is poisson's ration of the specimen, and E_i and ν_i are elastic constants of the indenter. Since $(1-\nu_i^2)/E_i$ is small compared to $(1-\nu^2)/E$, it is omitted. E_r of the diaphragm sample can be obtained by applying E values of either 1.35 MPa or 1.6 MPa obtained from curve fitting from Table 4.1. The values are smaller than the measured average value 3.76 MPa shown in Fig. 4.7 (b). This can be attributed to an increase in Young's modulus resulting from the loading tip touching locally agglomerated nickel particles.

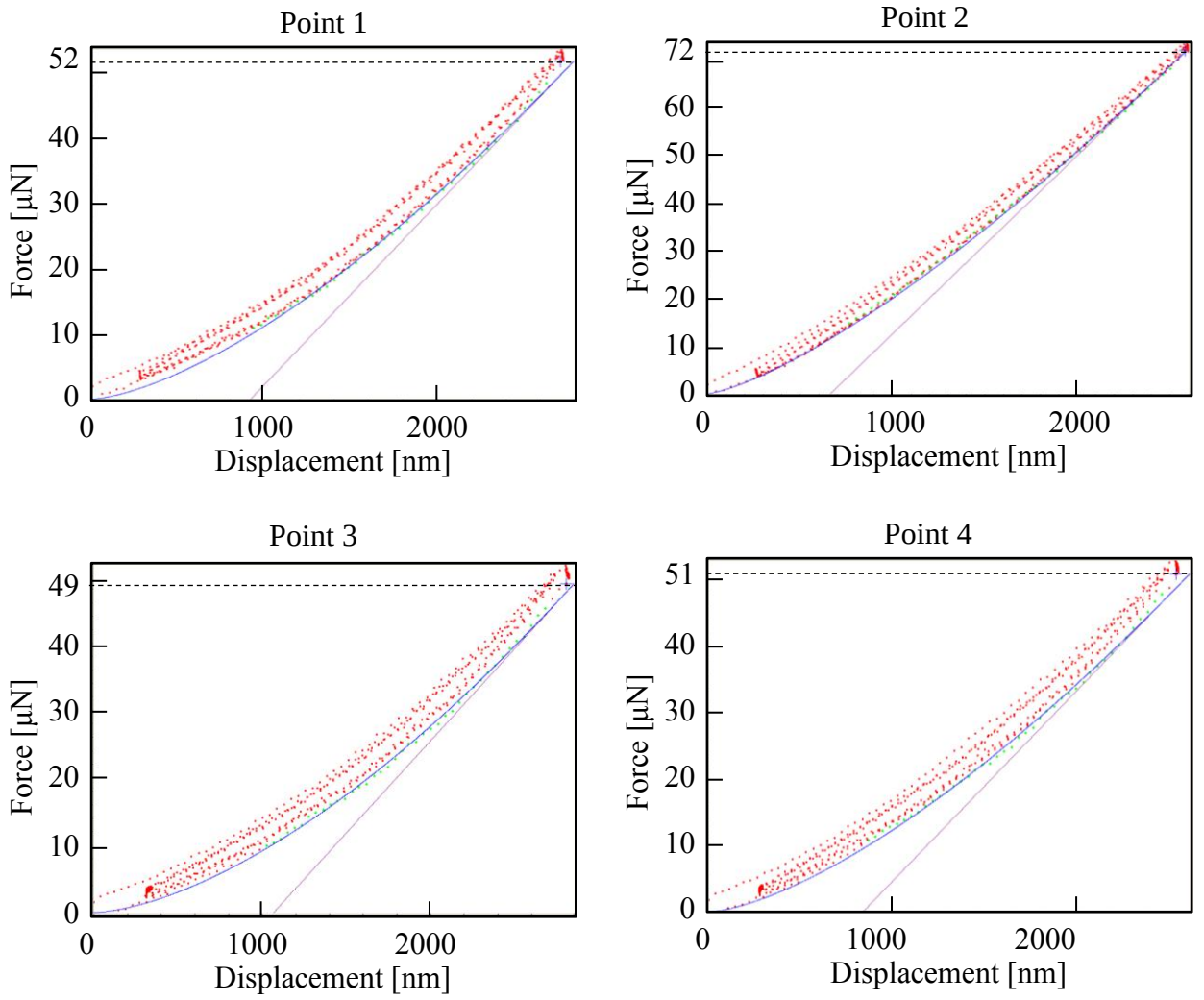

(a)

29.74 wt% PDMS/Ni-particle composite diaphragm						
Point	1	2	3	4	Av.	Thickness[μm]
E_r [MPa]	3.37	5.45	3.06	3.16	3.76	122
H [MPa]	0.97	1.95	0.77	0.94	1.15	

(b)

Fig. 4.7 Indentation measurements on PDMS/Ni-particle composite diaphragm (29.74 wt% of nickel). (a) Mechanical characteristic data and (b) data analysis of elasticity E_r and hardness H values for 29.74 wt% PNPC diaphragm.

4.2 MFSM Micropump Module for Hydrodynamic Focusing

Based on the results from the previous subsections, a hydrodynamic focusing module is fabricated and assembled. The goal is to achieve a change in fluid flow in a channel by controlling its stroke volume by applying magnetic field to the functionalized diaphragm and to suitably utilize this effect to achieve hydrodynamic focusing of flow through a channel.

The fabrication process starts with preparation of the bottom layer which consists of the chamber, Tesla-type valve, and all the inlets and the outlets. The next step is to cover the top of the bottom layer with the functionalized diaphragm containing submicron nickel particles, and to attach an air pressure inlet layer to the diaphragm chamber. In this fabrication, all bonding processes are done in oxygen plasma. In addition, permanent magnet is used for the prototype test structure to demonstrate the concept, and the magnet height can be manipulated by a threaded bolt. Figure 4.8 shows pictures of the fabricated device. The inlets and the outlet are connected by metal tubes through the PDMS and rubber tubes are connected to the metal tube endings. PDMS is additionally poured around the connecting holes to seal the device making it free of leaks.

Figure 4.9 displays the test setup for the MFSM micropump module. Two different colors of dyes are used for the test to color DI water red in the middle of the channel and green for the two outer edges of the channel. This is to help visualize channel flow during hydrodynamic focusing modulation. The device is mounted on the stage of a stereoscope, and video pictures are recorded by a CCD camera.

The flow rate is calculated based on the flow speed and the rubber tube diameter by the following equation:

$$V_{flowrate} = V_{velocity} \times A_{tube}. \tag{4.5}$$

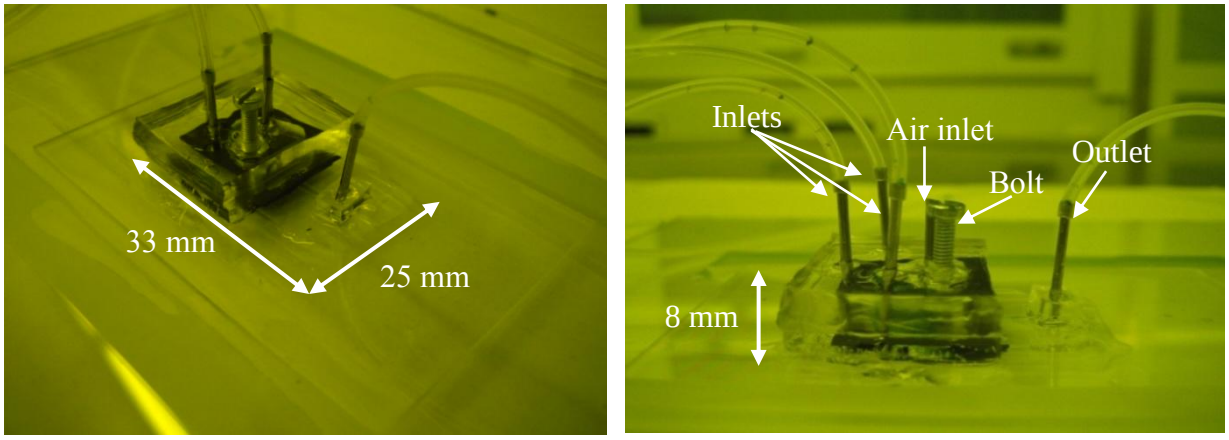

(a) (b)

Fig. 4.8 Pictures of the fabricated prototype MFSM micropump module. (a) Top view and (b) details of the feed-throughs for external connections.

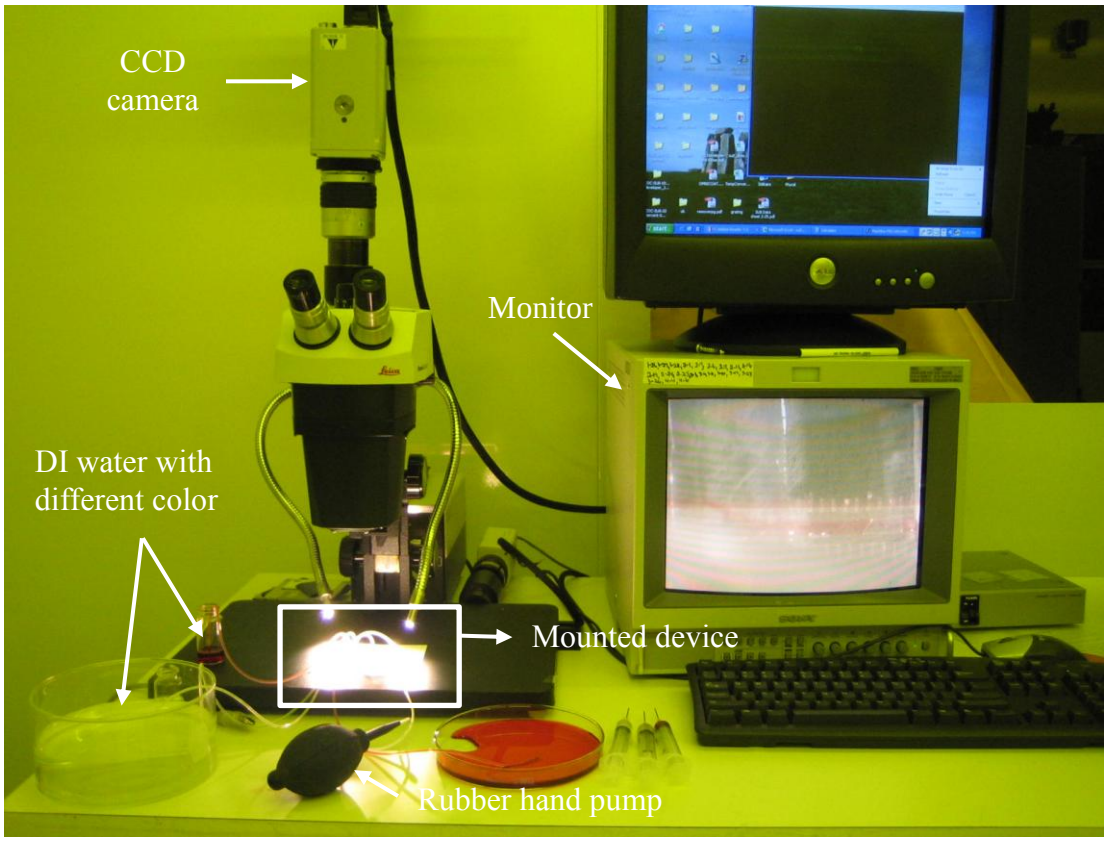

Fig. 4.9 The experimental setup for testing the MFSM micropump.

$V_{flowrate}$ is the flow rate of the dyed DI water solution in the tube, and A_{tube} is the cross sectional area of the round rubber tube, which has inner diameter of 1.65 mm. The measured $V_{velocity}$ is 2.5 mm/sec with a frequency of 2 Hz for the outlet tube. For this case, $V_{flowrate}$ is 321.13 µl/min. This flow rate is the total flow rate of three micropumps, so the flow rate of a single micropump is 107.04 µl/min, which is almost similar to the expected flow rate of 100 µl/min from the simulations.

Figure 4.10 illustrates the hydrodynamic focusing channel setup. The MFSM module is positioned under the optical microscope, and the lens is focused on the hydrodynamic channel. The image is transmitted to the monitor through a CCD camera during device operation. When the air pressure is applied to the diaphragm of the MFSM micropump, a certain stroke volume is generated by the diaphragm displacement which is shown in Fig. 4.11 (a). When the right permanent magnet approaches the PNPC diaphragm as sketched in Fig. 4.11 (b), the magnetic force working against the air pressure increases reducing the stroke volume on the right diaphragm. This result in a smaller flow on the right compared to the other diaphragms. Thus, the channel in the middle moves to the right side due to this stroke volume change.

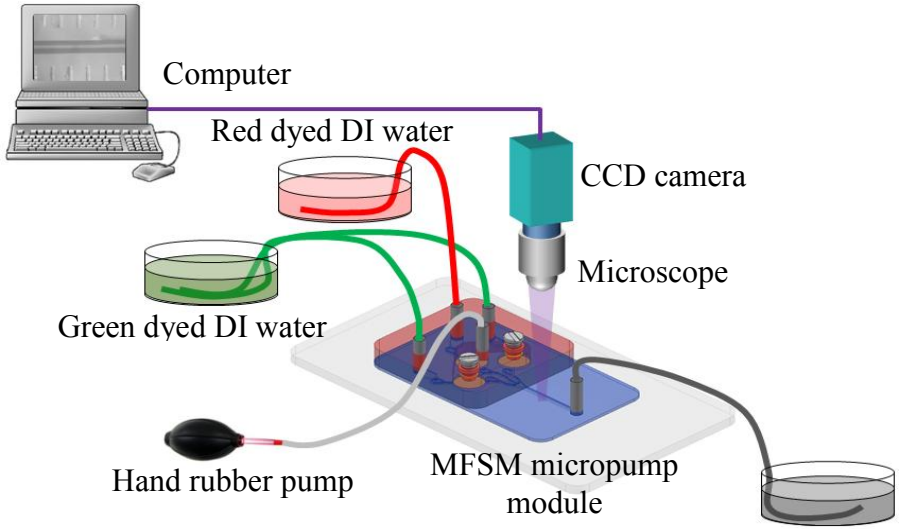

Fig. 4.10 MFSM micropump module test setup.

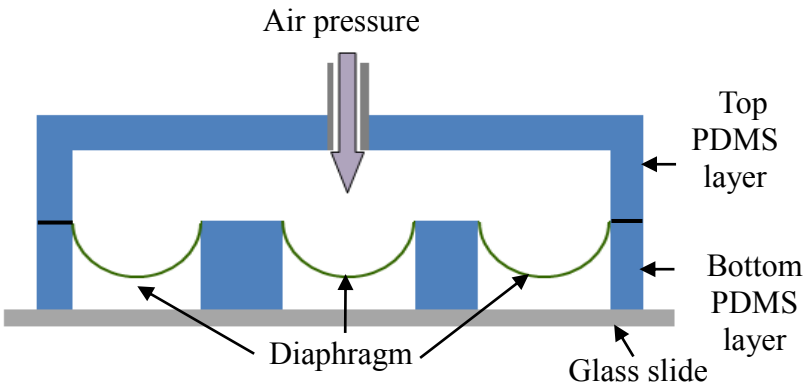

(a)

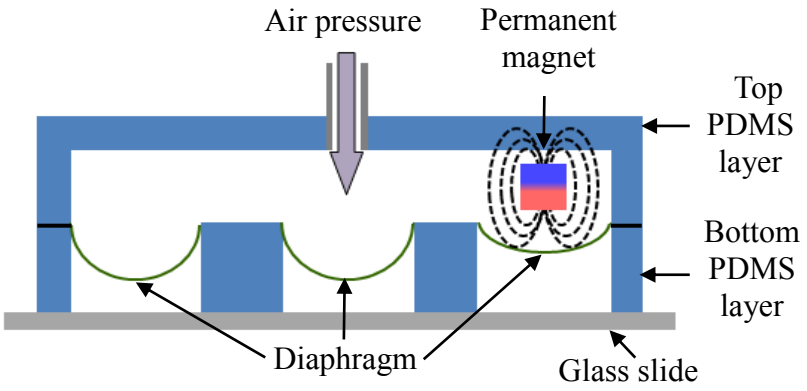

(b)

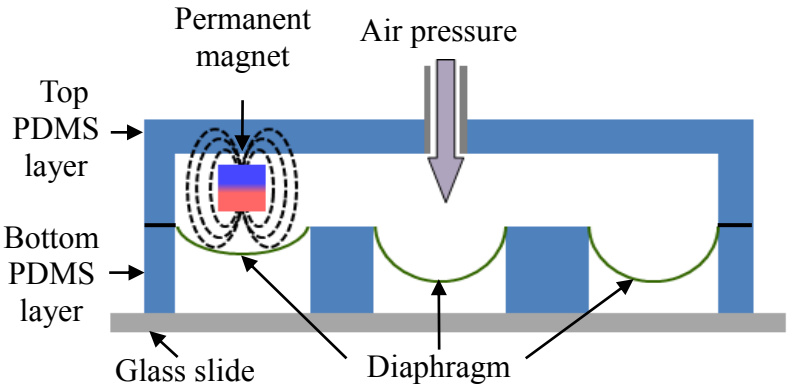

(c)

Fig. 4.11 The schematic of the hydrodynamic focusing channel modulation. (a) Middle focusing with no modulation, (b) right focusing with right diaphragm modulation, and (c) left focusing with left diaphragm modulation.

Figures 4.12 (a) and (b) show the images before and after modulation by the hydrodynamic focusing technique. The three micropumps are simultaneously operated by the air pressure source which in this test case is a hand rubber pump. Figure 4.12 (a) shows no channel modulation and the flow due to the center pump remains in the center with width of approximately 90 μm. In order to modulate the channel to the right of the flow direction, the permanent magnet associated with the right channel is lowered i.e. moved closer to the right channel PNPC diaphragm by moving the right side bolt closer, and the air pressure applied again. The middle channel now moves or focuses towards the right side of the channel because the right side pump stroke volume is reduced. The stroke volume on the left micropump remains large, so the larger amount of the left side solution pushes the middle channel to the right side. The right side channel width is now about 40 μm. Thus, the modulation by using the hydrodynamic focusing method has been demonstrated. The width of the middle channel in this case is reduced to 50 μm from 90 μm which is attributed to some trapped air bubbles in the middle chamber.

The center channel flow width can be varied by the PNPC diaphragm deflection which is changed by the relative position of the permanent magnet with respect to the diaphragm. Magnetic field on the diaphragm is measured by a Gauss/Tesla gauge as shown in Fig. 4.13. The maximum magnetic force is 130 mT with the direct contact to the magnet, and the magnetic field is reduced with distance.

Permanent magnet distance to PNPC diaphragm can modify the diaphragm displacement depending on the magnitude of the magnetic force acting on the latter. The modified diaphragm displacement is able to change the stream flow hence the stream width. The diaphragm displacement is achieved by the vertically moving permanent magnet which is connected to a

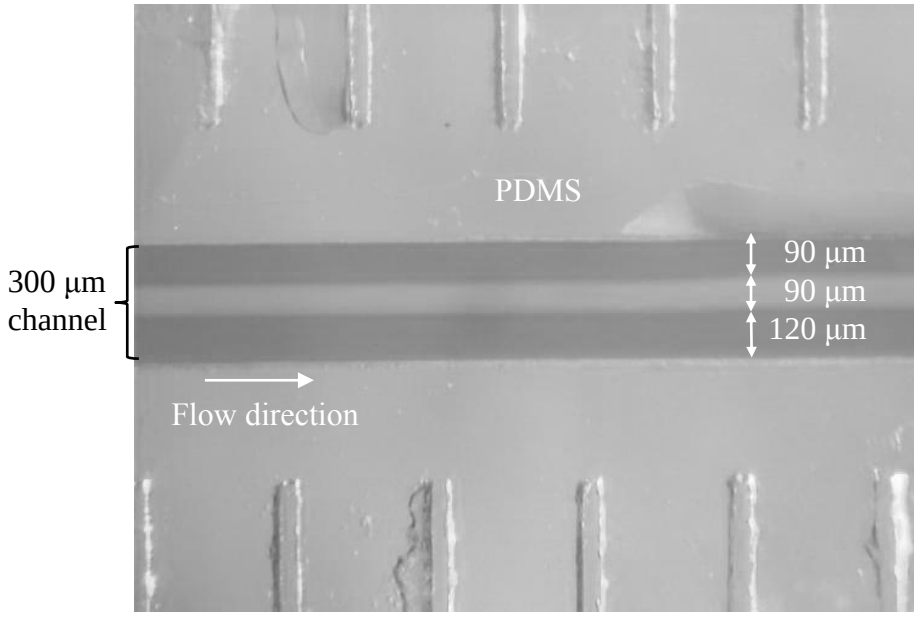

(a)

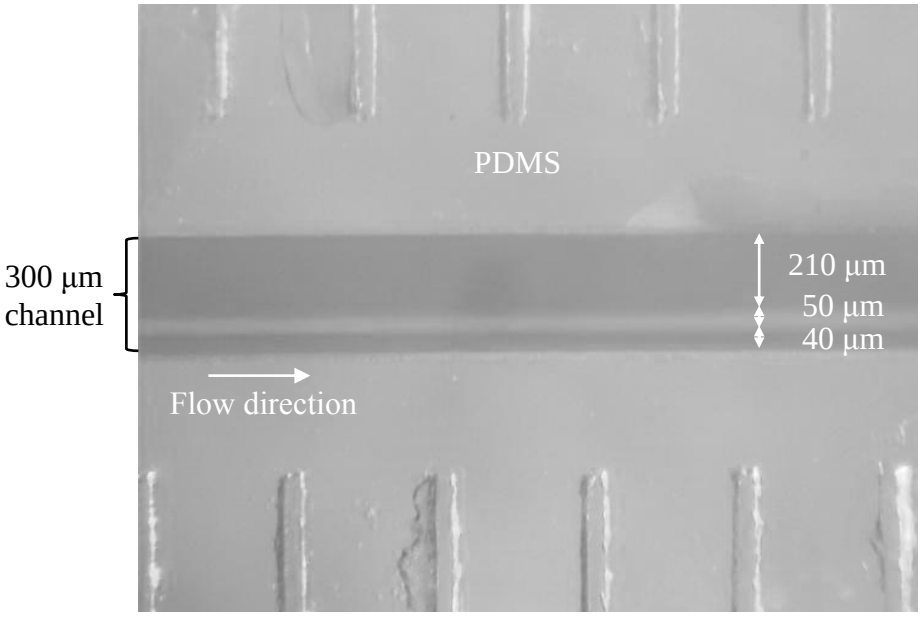

(b)

Fig. 4.12 Channel modulation by a magnetic force on the impregnated nickel particle diaphragm. (a) Middle focusing with no modulation and (b) right focusing with right diaphragm modulation.

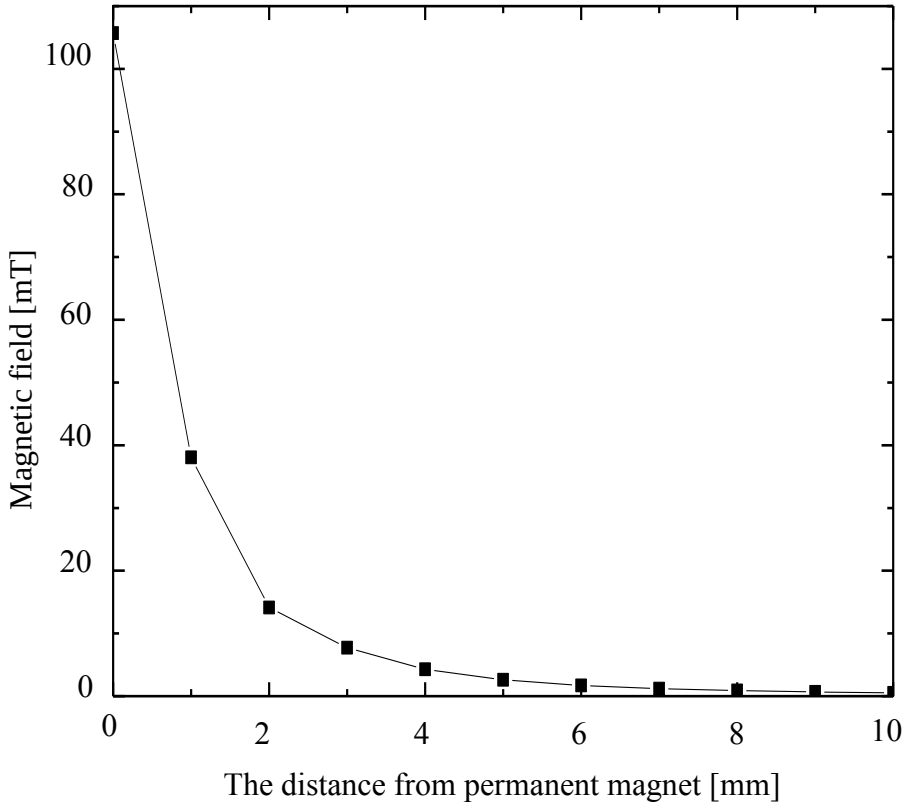

Fig. 4.13 Magnetic field as a function of vertical distance from the magnet center.

threaded bolt. The bolt moves vertically with a pitch of 500 μm/turn. Vertical movement from 250 μm to 3.5 mm can be achieved. The maximum deflection of the diaphragm is 190 μm with the magnet at a distance of 306 μm from the undeflected diaphragm position. The measured and calculated diaphragm displacements are compared in Fig. 4.14 as a function of the permanent magnet distance to undisplaced PNPC diaphragm. The calculated displacement values shown in Fig. 4.14 are obtained from the measured stream widths in the corresponding channel by varying the magnet position.

Table 4.2 gives the calculated diaphragm deflections with varying magnet position for only the right diaphragm side. The deflection values are calculated from the measured variation in width for each of the three flow streams given in Fig. 4.15. The middle and the left diaphragm channels have no magnets. The second column gives the right diaphragm up displacement as the

magnet position is varied due to attraction. The last three columns in Table 4.2 give the three diaphragm displacements when the magnet position is varied on the right diaphragm under approximate average 1.8 kPa air pressure with the hand rubber pump. Note that the left and the middle diaphragm displacement increase with decreasing magnet distance on the right diaphragm due to a slight increase in pressure in the chamber caused by a decrease in chamber volume resulting from the right diaphragm displacement under changing magnetic force field. In addition, Fig. 4.15 indicates channel width modulations with different magnet positions over the right diaphragm. The stroke volume of the diaphragm is calculated from the experimental observation of the hydrodynamic focusing channel width change. The stroke volume is changed by the permanent magnet distance to the functionalized right diaphragm as evidenced from Table 4.2. The channel widths of the three flows are changed by the stroke volume variations for the three streams. In Fig. 4.15 L, M, and R respectively represent the left, the middle, and the right channels. Right diaphragm is the only one interacting with the permanent magnet in these measurements.

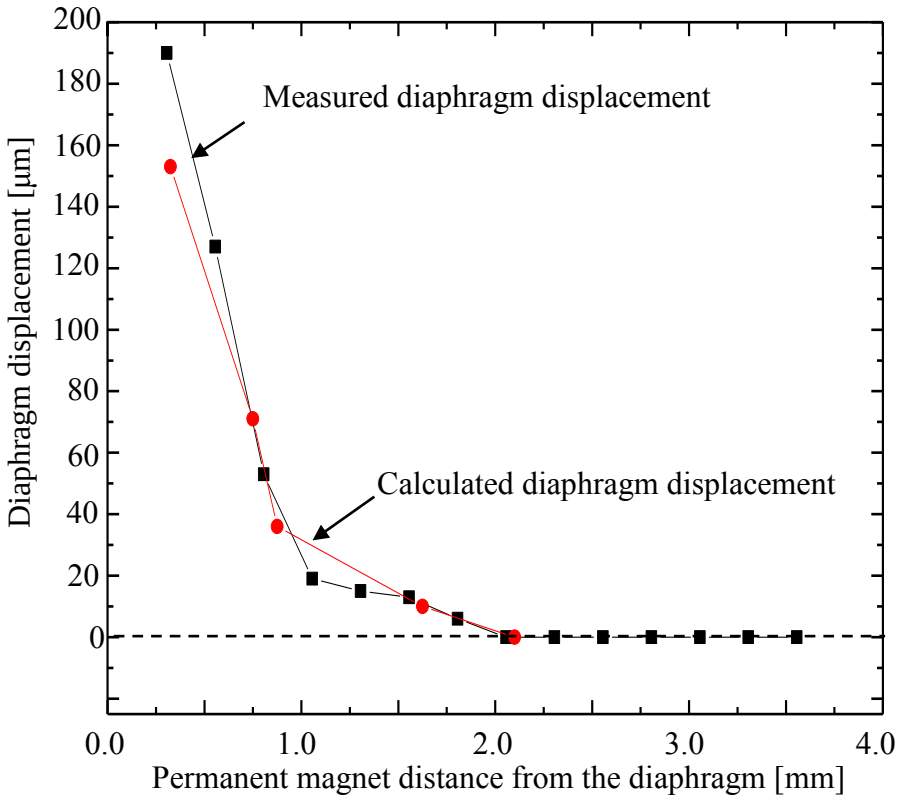

Fig. 4.14 The PNPC diaphragm displacement by the permanent magnet as a function of the magnet distance from the top of the cover layer to the diaphragm with the approximate average 1.8 kPa applied air pressure.

Table 4.2 The PNPC diaphragm (left, middle and right) displacement as a function of the permanent magnet distance from the top of the cover layer to the undisplaced diaphragm under approximate average 1.8 kPa air pressure.

The distance from the permanent magnet to PNPC diaphragm [mm]	Right diaphragm up displacement by permanent magnet without air pressure [μm]	Diaphragm down displacement on the left channel with respect to air pressure [μm]	Diaphragm down displacement on the middle channel with respect to air pressure [μm]	Diaphragm down displacement on the right channel with respect to air pressure [μm]
≥ 2.1	0	305	208	296
1.625	10	314	246	286
0.875	36	330	215	260
0.750	71	322	265	225
0.375	153	346	272	143

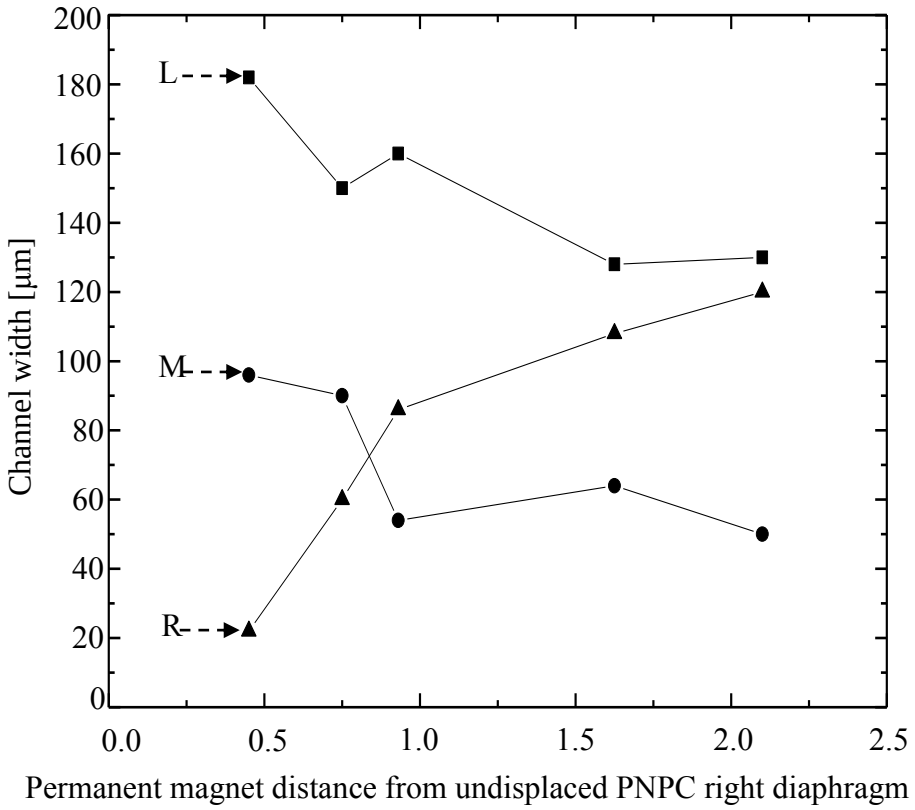

Fig. 4.15 Measured channel width variations resulting from permanent magnet distance variation from the undisplaced PNPC right diaphragm for approximate average 1.8 kPa air pressure.

CHAPTER 5

SUMMARY, CONCLUSION, AND SUGGESTIONS FOR FUTURE WORK

5.1 Summary and Conclusions

Micro total analysis system (μTAS) and lab-on-a-chip (LOC) research community has grown over the last several decades and the market for microfluidics industry is estimated to be between $3 billion to $4.5 billion with the growth rate of about 25 to 35 percent as reported by the System Planning Corporation [22]. Many areas in the microfluidics field such as micromixers, microvalves, and micropumps have been investigated. Among them, micropump is among the more interesting components for μTAS and LOC. Efficiency enhancement in cost and performance for micropumps is important for further rapid development of μTAS and LOC.

Technology to modulate the stream flow by hydrodynamic focusing is studied in this research for possible applications in μTAS and LOC. Modulating hydrodynamically focused stream flow in a channel can be achieved by a new type of micropump called multi-fluidic speed-modulating (MFSM) micropump. The benefits of MFSM micropump for μTAS and LOC include reduction in fabrication cost and an increase in sensing performance by employing a wide channel and achieving a means to hydrodynamically focus the flow stream. Small channels are preferred since they require a small amount of sample volume as the overall device sizes are reduced. However, the chip alignment issues get difficult or expensive with small sized channels. Precise channel alignment causes increasing fabrication cost. In addition, a narrow single channel is not suitable for most μTAS and LOC utilizing cells as a sample because of cell-clogging and agglomeration in the channel. Hence, hydrodynamic focusing method with three micropumps as carried out in this work is a better approach.

The challenges to build a prototype of the MFSM micropump to enable hydrodynamical focusing of fluid stream flow and channel width modulation are addressed here. A pneumatic actuating method is adapted to generate sufficient force for the reciprocating micropump. The diaphragm for the micropump is functionalized with PDMS/Ni-particle composite which interacts with vertical magnetic force in order to modulate the diaphragm displacement against the pneumatic force. Chamber design and valve shape are considered to optimize the flow rate. Computational modeling is utilized for simulation to achieve at a suitable prototype micropump design in chapter 2. Design flexibility with changing parameters, is also described in chapter 2.

Based on the simulation results, the components of the prototype MFSM micropump are fabricated. The micropump comprises of three layers: the top air source inlet layer, the middle PDMS/Ni-particle composite diaphragm layer, and the bottom chamber and the valve layer. During fabrication, the PDMS top and bottom layers are casted from a master mold, and the functionalized diaphragm in the middle is fabricated by spin-coating a mixture of a PDMS polymer with submicron nickel particles. All processes mentioned here are described in chapter 3.

The fabricated PNPC diaphragm's Young's modulus is measured on a test setup, and the results are compared with the mechanical properties measurement by indentation technique. All layers of the MFSM micropump are assembled for a functional test of the prototype design. Hydrodynamically focused flow stream is created for modulating channel flow by three individual micropumps operating simultaneously. The total measured flow rate of the three MFSM micropumps was 321.13 μl/min at a frequency of 2 Hz. The flow rate of the individual micropump is about 107.04 μl/min. The hydrodynamically focused channel flow can be modulated by changing permanent magnet distance from the PNPC diaphragm, which changes stroke volume of the diaphragm. The middle channel, which includes the test sample, can be

modulated either left or right side of the channel center by changing the magnet distances. This research demonstrates the potential of MFSM micropump for modulating a channel flow by hydrodynamic focusing achieved by applying a magnetic force to the functionalized diaphragm. The position and width of the streams can be changed by changing magnet distance to the diaphragm under an applied air pressure. A closer magnet position to the diaphragm causes a larger stream change in both position and width of the flow. Under approximate average 1.8 kPa air pressure, the right channel varies from 120 μm to below 30 μm when the magnet height is varied from greater than 2.1 mm to 0.375 mm.

MFSM micropump for hydrodynamic focusing for μTAS and LOC application has several potential benefits. First, a wider channel reduces fabrication cost compared to a narrower channel. A wider channel can be used with hydrodynamic focusing method because the flow width in the channel can be controlled by the flow rate of two other buffer solutions. It is possible to make a narrow channel width by changing the flow rates of the two adjoining channels. Second, the reduced channel width provides higher possibility to improve sensitivity for reaction between a particular cell in the sample flow and specific targets located in the channel such as functionalized nanostructures. Third, hydrodynamic focusing method can protect cell clogging in a channel because the two buffer solutions at right and left sides isolate the middle flow from the direct contact to the channel walls.

5.2 Suggestions for Future Work

MFSM micropump proposed in this research provides the advantages listed in the last section for μTAS and LOC applications. The fluidic control unit of the module as proposed here is much smaller than the conventional pump to realize hydrodynamic focusing. It can control the

flow rate by simple manipulation since the diaphragm of the MFSM micropump is mainly actuated by air pressure and the magnet manipulates the diaphragm displacement. However, there are some issues such as diaphragm material, use of a permanent magnet, actuation method, and hot embossing technique which need further improvement and consideration for enhancing the MFSM micropump performance.

One of the important parts in a MFSM micropump is the diaphragm impregnated with nickel particles. Submicron nickel particles make the polydimethylsiloxane (PDMS) diaphragm functionalized to interact with the magnetic field. However, increasing the density of the nickel particles can cause severe agglomeration on the diaphragm. Therefore, the density and thickness of the diaphragm should be optimized.

In order to manipulate the diaphragm displacement, permanent magnet is an essential part of the MFSM micropump, but the magnetic force cannot be accurately controlled by manually locating permanent magnet towards the functionalized diaphragm. An effective method to precisely control magnetic force needs to be developed. Solenoid, a simple electromagnet, has the potential, because the magnetic force can be easily and precisely modified by controlling the current. However, solenoid design to generate high magnetic field has several fabrication issues including the volume consideration and heat generation. Though the magnetic field can be increased by increasing the number of turns, it makes the solenoid bulky and increases the coil resistance. Longer wire length requires higher driving voltage for solenoid and generates greater amount of heat because of the increased wire resistance for a given magnitude of current. If the voltage is reduced to decrease generated heat, the current is also decreased, and the solenoid cannot generate enough magnetic fields to lift the PNPC diaphragm. Therefore, building a solenoid with reduced heat generation or improved heat dissipation is an important objective.

While conducting tests on the MFSM micropump for modulating the channel flow, a rubber hand pump was used to manually apply air pressure to the diaphragm. The pumping frequency was about 2 Hz. In order to optimize MFSM micropump performance, a variety of frequency ranges need to be applied.

In our work here, PDMS has been utilized so far for making the top and the bottom layers. Futher work should investigate other materials. For example hot embossing is an efficient replication technique to make high quality microfluidic devices using materials such as PMMA [26]. The hot embossing machine has a mold mounting stage and a vacuum chamber. Figure 5.1 (a) shows the brass mold of MFSM micropump on the mounting stage. The inserted mold presses thin plastic sheet around the glass transition temperature under vacuum. In this research, 1.5 mm thick PMMA sheets and a molding temperature of about 160 ℃ have been used to investigate use of PMMA for the MFSM micropumps. The inset pattern is transferred onto a PMMA sheet in 20 minutes. The replication result from the mold inset is shown in Fig. 5.1 (b). Better quality structures are obtained by accurate control of the temperature and the force in order to reduce thermal stress. The structural views of MFSM micropump module are shown in Fig. 5.2. The entire structural view is in Fig. 5.2 (a), and Tesla-type valve, hydrodynamic focusing zone, and chamber are displayed respectively in Figs. 5.2 (b), (c) and (d). Future work should include operating MFSM micropump fabrication from other polymers such as PMMA.

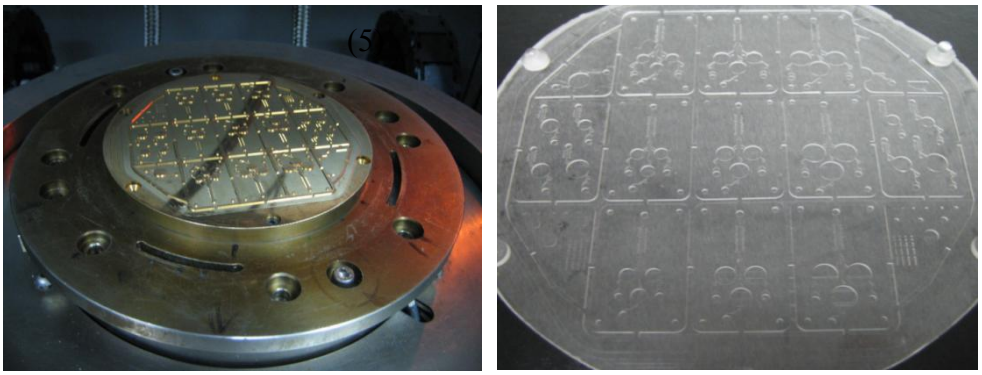

(a) (b)

Fig. 5.1 Hot embossing process with (a) brass mold insert mounted and (b) PMMA wafer of MFSM micropump obtained after hot embossing.

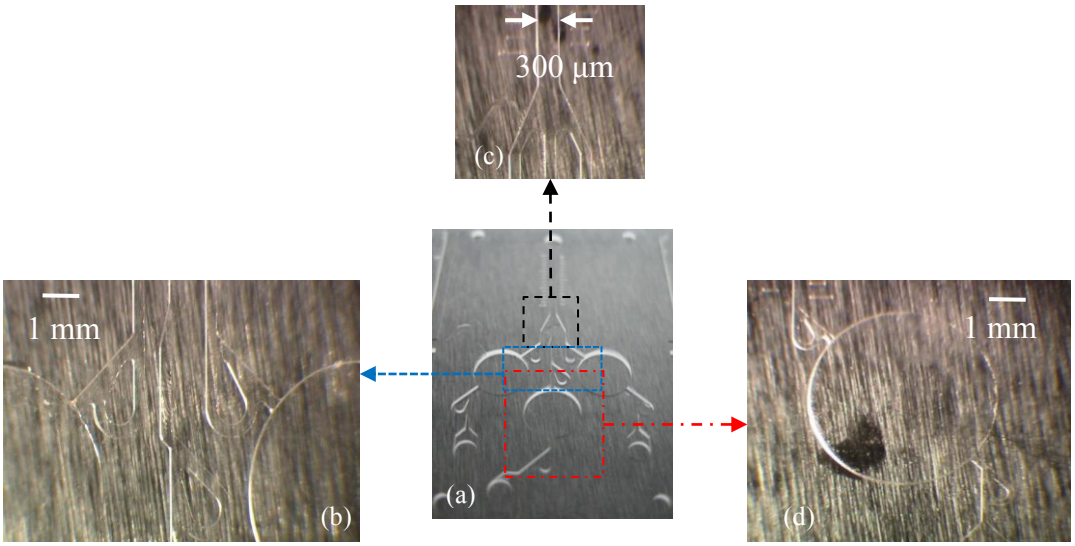

Fig. 5.2 Structural views of MFSM micropump made in PMMA.

REFERENCES

[1] L. Kang, B. G. Chung, R. Langer and A. Khademhosseini, Microfluidics for drug discovery and development: From target selection to product lifecycle management," Drug Discovery Today, 13 (1/2), p1 (2008).

[2] G. M. Whitesides, "The origins and the future of microfluidics," Nature, 442 (7101), p368 (2006).

[3] S. Haeberle and R. Zengerle, "Microfluidic platforms for lab-on-a-chip applications," Lab on a Chip, 7 (9), p1094 (2007).

[4] P. Gravesen, J. Branebjerg and O. S. Jensen, "Microfluidics-a review," Journal of Micromechanics and Microengineering, 3 (4), p168 (1993).

[5] C. P. Price, A. St. John and J. M. Hicks, *Point-of-care testing*, 2nd edition (American Association for Clinical Chemistry Press, 2004).

[6] C.-L. Choong, W. I. Milne and K. B. K. Teo, "Review: carbon nanotube for microfluidic lab-on-a-chip application," International Journal of Material Forming, 1 (2), p117 (2008).

[7] F. Patolsky, G. Zheng and C. M. Lieber, "Nanowire-based biosensors," American Chemical Society, 78 (13), p4261 (2006).

[8] D. R. Reyes, D. Iossifidis, P.-A. Auroux and A. Manz, "Micro total analysis systems. 1. introduction, theory, and technology," Analytical Chemistry, 74 (12), p2623 (2002).

[9] N.-C. Tsai and C.-Y. Sue, "Review of MEMS-based drug delivery and dosing systems," Sensors and Actuators A: Physical, 134 (2), p555 (2007).

[10] A. Nisar, N. Afzulpurkar, B. Mahaisavariya and A. Tuantranont, "MEMS-based micropumps in drug delivery and biomedical applications," Sensors and Actuators B: Chemical, 130 (2), p917 (2008).

[11] J. Haynes, "J. Frost & Sullivan: Point-of-Care Testing Market Finds Expanded Opportunities With Higher End-User Demand," (2009); Available from: http://www.prnewswire.com/news-releases/frost--sullivan--point-of-care-testing-market-finds-expanded-opportunities-with-higher-end-user-demand-90929669.html.

[12] H. Suzuki and R. Yoneyama, "Integrated microfluidic system with electrochemically actuated on-chip pumps and valves," Sensors and Actuators B: Chemical, 96 (1-2), p38 (2003).

[13] A. Puntambekar and C. H. Ahn, "Self-aligning microcluidic interconnects for glass- and plastic-based microfluidic systems," Journal of Micromechanics and Microengineering, 12 (1), p35 (2002).

[14] P. K. Sorger, "Microfluidics closes in on point-of-care assays," Nature Biotechnology, 26 (12), p1 (2008).

[15] H.-T. Changa, C.-Y. Leea, C.-Y. Wen and B.-S. Hong, "Theoretical analysis and optimization of electromagnetic actuation in a valveless microimpedance pump," Microelectronics Journal, 38 (6-7), p791 (2007).

[16] S. Zheng, R. Yung, Y.-C. Tai and H. Kasdon, "Determinstic lateral displacement MEMS device for continuous blood cell separation," Micro Electro Mechanical Systems, 18th IEEE International Conference, p851, January (2005).

[17] N. Frische, P. Datta and J. Goettert, "Development of a biological detection platform utilizing a modular microfluidic stack," Microsystem Technologies, 16 (8-9), p1553 (2010).

[18] J. Döppery, M. Clemens., W. Ehrfeld, S. Jung, K.-P. Kämper and H. Lehr, "Micro gear pumps for dosing of viscous fluids," Journal of Micromechanics and Microengineering,7, p230 (1997).

[19] W. C. Young and R. G. Budynas, *Roark's Formulas for Stress and Strain*, 7th edition, (McGraw-Hill 2002).

[20] D. J. Laser and J. G. Santiago, "A review of micropumps," Journal of Micromechanics and Microengineering,14 (6), pR35 (2004).

[21] A. C. Balazs, T. Emrick and T. P. Russell, "Nanoparticle polymer composites: where two small worlds meet," Science, 314 (17), p1107 (2006).

[22] N.-T. Nguyen, X. Huang and T. K. Chuan, "MEMS-micropumps: a review," Journal of Fluids Engineering, 124 (2), p384 (2002).

[23] M. Koch, N. Harris, A. G. R. Evans, N. M. White and A. Brunnschweiler, "A novel micromachined pump based on thick-film piezoelectric actuation," Sensors and Actuators A: Physical, 70 (1-2), p98 (1998).

[24] S. Shoji and M. Esashi, "Microflow devices and systems," Journal of Micromechanics and Microengineering, 4 (4), p157 (1994).

[25] E. Stemmea and G. Stemme, "A valveless diffuser/nozzle-based fluid pump," Sensors and Actuators A: Physical, 39 (2), p159 (1993).

[26] B. D. Iverson and S. V. Garimella, "Recent advances in microscale pumping technologies: a review and evaluation," Microfluidics and Nanofluidics, 5 (2), p145 (2008).

[27] A. R. Gamboa, C. J. Morris and F. K. Forster, "Improvements in fixed-valve micropump performance through shape optimization of valves," Journal of Fluids Engineering, 127 (2), p339 (2005).

[28] A. R. Gamboa and F. K. Forster, "Is there a best fixed-geometry valve for micropumps?," 2004 ASME International Mechanical Engineering Congress and RD&D Expo, p1, November (2004).

[29] H.-T. Chang, C.-Y Wen and C.-Y. Lee, "Design, analysis and optimization of an electromagnetic actuator for a micro impedance pump," Journal of Micromechanics and Microengineering, 19 (8), p1 (2009).

[30] X. N. Jiang, Z. Y. Zhou, X. Y. Huang, Y. Li, Y. Yang and C. Y. Liu, "Micronozzle/diffuser flow and its application in micro valveless pumps," Sensors and Actuators A: Physical, 70 (1-2), p81 (1998).

[31] F. Pirmoradi, L. Cheng and M. Chiao, "A magnetic poly(dimethylesiloxane) composite membrane incorporated with uniformly dispersed, coated iron oxide nanoparticles," Journal of Micromechanics and Microengineering, 20 (1), p1 (2010).

[32] S. Bhattacharya, A. Datta, J. M. Berg, and S. Gangopadhyay, "Studies on surface wettability of poly(dimethyl) siloxane (PDMS) and glass under oxygen-plasma treatment and correlation with bond strength," Journal of Microelectromechanical Systems, 14 (3), p590 (2005).

[33] A. L. Thangawng, R. S. Ruoff, M. A. Swartz and M. R. Glucksberg, "An ultra-thin PDMS membrane as a bio/micro–nano interface: fabrication and characterization," Biomedical Microdevices, 9 (4), p587 (2007).

[34] W. C. Oliver and G. M. Pharr, "Measurement of hardness and elastic modulus by instrumented indentation: Advances in understanding and refinements to methodology," Journal of Materials Research, 19 (1), p3 (2003).

[35] W. C. Oliver and G. M. Pharr, "An improved technique for determining hardness and elastic modulus using load and displacement sensing indentation experiments," Journal of Materials Research, 7 (6), p1564 (1992).

VITA

Jeonghwan Kim was born in Pusan, South Korea, in 1980. He graduated with his Bachelor of Science degree (2007) in electrical engineering from Kyungwon University, S. Korea. Between 2007 and 2008, he did graduate work in electrical engineering at Arizona State University, Tempe, Arizona.

In 2009, he transferred to Louisiana State University, Baton Rouge, Louisiana. During his graduate research, he worked on the development of a prototype for in-situ tunable hydrodynamic focusing module driven with three multi-fluidic speed modulating (MFSM) micropumps for microfluidic applications.

He also worked as a research assistant in the Center for Advanced Microstructures and Devices (CAMD) at Louisiana State University, and worked on the development of microfluidic chips and on X-ray lithography process for BioMEMS.